



City Research Online

City, University of London Institutional Repository

Citation: Castro-Alvaredo, O., Lencsés, M., Szécsényi, I. M. & Viti, J. (2020). Entanglement Oscillations near a Quantum Critical Point. *Physical Review Letters*, 124(23), pp. 1-7. doi: 10.1103/physrevlett.124.230601

This is the accepted version of the paper.

This version of the publication may differ from the final published version.

Permanent repository link: <https://openaccess.city.ac.uk/id/eprint/24874/>

Link to published version: <https://doi.org/10.1103/physrevlett.124.230601>

Copyright: City Research Online aims to make research outputs of City, University of London available to a wider audience. Copyright and Moral Rights remain with the author(s) and/or copyright holders. URLs from City Research Online may be freely distributed and linked to.

Reuse: Copies of full items can be used for personal research or study, educational, or not-for-profit purposes without prior permission or charge. Provided that the authors, title and full bibliographic details are credited, a hyperlink and/or URL is given for the original metadata page and the content is not changed in any way.

City Research Online:

<http://openaccess.city.ac.uk/>

publications@city.ac.uk

Entanglement Oscillations near a Quantum Critical Point

Olalla A. Castro-Alvaredo,¹ Máté Lencsés,^{2,3} István M. Szécsényi,⁴ and Jacopo Viti^{5,6}

¹*Department of Mathematics, City, University of London,
10 Northampton Square, EC1V 0HB London, UK*

²*BME Department of Theoretical Physics, H-1111 Budapest, Budafoki út 8.*

³*BME “Momentum” Statistical Field Theory Research Group, H-1111 Budapest, Budafoki út 8.*

⁴*Nordita, KTH Royal Institute of Technology and Stockholm University,
Roslagstullsbacken 23, SE-106 91 Stockholm, Sweden*

⁵*International Institute of Physics & ECT, UFRN,
Campos Universitário, Lagoa Nova 59078-970 Natal, Brazil*

⁶*INFN, Sezione di Firenze, Via G. Sansone 1, 50019 Sesto Fiorentino, Firenze, Italy*

(Dated: June 15, 2020)

We study the dynamics of entanglement in the scaling limit of the Ising spin chain in the presence of both a longitudinal and a transverse field. We present analytical results for the quench of the longitudinal field in critical transverse field which go beyond current lattice integrability techniques. We test these results against a numerical simulation on the corresponding lattice model finding extremely good agreement. We show that the presence of bound states in the spectrum of the field theory leads to oscillations in the entanglement entropy and suppresses its linear growth on the time scales accessible to numerical simulations. For small quenches we determine exactly these oscillatory contributions and demonstrate that their presence follows from symmetry arguments. For the quench of the transverse field at zero longitudinal field we prove that the Rényi entropies are exactly proportional to the logarithm of the exponential of a time-dependent function, whose leading large-time behaviour is linear, hence entanglement grows linearly. We conclude that, in the scaling limit, linear growth and oscillations in the entanglement entropies can not be simply seen as consequences of integrability and its breaking respectively.

Introduction.— Over the past two decades, one-dimensional many-body quantum systems far from equilibrium have become ubiquitous laboratories to scrutinize fundamental aspects of statistical mechanics. Out-of-equilibrium protocols featuring unitary dynamics, such as quantum quenches, have been commonly employed to test relaxation and thermalization hypothesis [1, 2] in experimentally realizable setups [3–6]. A powerful theoretical device that tests whether a physical system can eventually approach equilibrium is represented by its entanglement dynamics [7]. In 1+1 dimensions, the linear-in-time increase of the entanglement entropies is a signature that local observables relax exponentially fast [8–10] and thermalize [11, 12]. This characteristic growth has been further conjectured to be a generic feature of integrable models [13], where it has been analyzed within a quasi-particle picture, inspired by conformal field theory [7] and free fermion calculations [14]. In such a framework, entangled quasi-particle pairs propagate freely in space-time and generate linearly growing entropies. Minimal models, with random unitary dynamics, that show analogous entanglement growth, have been also studied [15, 16] in connection with quantum chaos [17, 18] and non-integrable systems.

Nonetheless, there exist a vast class of one-dimensional systems that escape this paradigm and fail to relax at large times after the quench. They have been observed both in earlier studies [19] and in actual recent experiments [20], see also [21]. Within a qualitative quasi-particle picture [22], absence of thermalization has

been associated with integrability breaking interactions and confinement. Numerical studies in the Ising spin chain [22] and its scaling limit [23–26] indicated that in the presence of a longitudinal field entanglement growth is strongly suppressed while local observables feature persistent oscillations whose frequencies coincide with the meson masses. A similar lack of relaxation has been also found later in a variety of physical models spanning from gauge theories [27–30] and fractons [31] to Heisenberg magnets [32] and systems with long-range interactions [33]. However, despite a large number of numerical investigations, most of the understanding of whether and how local observables will equilibrate after a quench remains at a phenomenological level. This is mainly because no lattice integrability technique [34] is available to systematically analyze these strongly interacting systems.

In this Letter, we put forward a unified picture to address perturbatively questions about entanglement dynamics and relaxation in gapped 1+1 dimensional systems close to a Quantum Critical Point (QCP). In particular, for the first time, we provide an analytical grasp on how entanglement growth can be so dramatically different depending on the non-equilibrium protocol considered. The formalism combines the perturbative approach of [35, 36] with the mapping in the scaling limit between powers of the reduced density matrix and correlation functions of a local field, called the branch point twist field [37, 38]. For massive systems, this mapping has been successfully employed at equilibrium [39] and

recently also in a time-dependent context [40]. Crucially, its conclusions do not rely on any *a priori* assumption about the space-time evolution of the quasi-particles.

Focussing on the illustrative example of a quench of the longitudinal field in the ferromagnetic Ising spin chain, we will provide examples of how bound state formation and symmetries of the twist field are responsible for slow relaxation of local observables and oscillations in the entanglement entropies. Although derived through field theory techniques our results are tested numerically in the lattice model in the scaling limit and very good agreement is found.

Model.— Consider the ferromagnetic Ising spin chain defined by the Hamiltonian

$$H_{\text{lattice}} = - \sum_{n \in \mathbb{Z}} [\sigma_n^x \sigma_{n+1}^x + h_z \sigma_n^z + h_x \sigma_n^x]. \quad (1)$$

The Ising chain is a prototype of a quantum phase transition with spontaneous breaking of \mathbb{Z}_2 symmetry and is critical for $h_z = 1$ and $h_x = 0$. At criticality, the low energy excitations are massless free Majorana fermions described by a conformal field theory with central charge $c = 1/2$ [41]. Within the renormalization group framework, near the QCP, expectation values of local operators in the spin chain can be calculated from the relativistic Quantum Field Theory (QFT) action

$$\mathcal{A}_0 = \mathcal{A}^{\text{CFT}} - \lambda_1 \int dx dt \varepsilon(x, t) - \lambda_2 \int dx dt \sigma(x, t), \quad (2)$$

which is the celebrated Ising field theory (IFT) [42–44]. In Eq. (2), the conformal invariant action \mathcal{A}^{CFT} is perturbed by the \mathbb{Z}_2 even field ε (energy), which is the continuum version of the lattice operator σ_n^z , and the \mathbb{Z}_2 odd field σ (spin), which is instead the continuum version of the order parameter σ_n^x . The coupling constant λ_1 is proportional to the deviation of the transverse field from its critical value $h_z - 1$, while λ_2 is proportional to the longitudinal field h_x . At the QCP, the scaling dimension of σ is $\Delta_\sigma = 1/8$ and that of ε is $\Delta_\varepsilon = 1$.

Let $|\Omega\rangle$ be the ground state of the Hamiltonian H of the field theory (2). Following a widely studied non-equilibrium protocol, dubbed *quantum quench*, at time $t = 0$ one of the two coupling constants λ_i ($i = 1, 2$) is modified according to $\lambda_i \rightarrow \lambda_i + \delta\lambda$. The evolution of the pre-quench ground state $|\Omega\rangle$ is governed by the perturbed Hamiltonian

$$G(t) := H + \theta(t)\delta\lambda \int dx \Psi(x), \quad (3)$$

Ψ being either the spin or the energy field and $\theta(t)$, the Heaviside step function. This dynamical problem is analytically not solvable in general [35]. To provide theoretical predictions for local observables and entanglement entropies following a quench, one thus sets up a perturbative expansion in the relative quench parameter $\frac{\delta\lambda}{\lambda_i} \ll 1$.

Perturbation Theory.— We revisit and extend to include entanglement calculations, the perturbative approach to the quench problem [35]. In a relativistic scattering theory, it is possible to consider a basis of in and out states, denoted by $|\alpha\rangle^{\text{in/out}}$, which are multi-particle eigenstates of the Hamiltonian $H = G(-\infty)$. In particular, a single-particle eigenstate of H has energy $e(p) = \sqrt{m_0^2 + p^2}$, where m_0 is its pre-quench mass and p the momentum. Similar eigenbases are constructed for the post-quench Hamiltonian $H_{\text{post}} := H + \delta\lambda \int dx \Psi(x) = G(\infty)$. In this case, the energy of a single-particle state will be denoted by $\tilde{e}(p) = \sqrt{m^2 + p^2}$, being m its post-quench mass.

The initial state $|\Omega\rangle$ can be formally expanded into the basis of the out-states of H_{post} as: $|\Omega\rangle = \sum_\alpha c_\alpha |\alpha\rangle_{\text{post}}^{\text{out}}$. Assuming for simplicity a unique family of particles, $|\alpha\rangle_{\text{post}}^{\text{out}}$ is then the multiparticle out-state $|p_1, \dots, p_n\rangle_{\text{post}}^{\text{out}}$ while the symbol \sum_α is a shorthand notation for the Lorentz invariant integration measure in 1+1 dimensions [47]. The overlap coefficients c_α are the elements of the scattering matrix for the quench problem in Eq. (3). At first-order in perturbation theory, one has [45, 46]

$$|\Omega\rangle = |\Omega\rangle_{\text{post}} + 2\pi\delta\lambda \sum_{\alpha \neq \Omega} \frac{\delta(P^\alpha)}{E^\alpha} (F_\alpha^\Psi)^* |\alpha\rangle_{\text{post}}^{\text{out}} + \mathcal{O}(\delta\lambda^2). \quad (4)$$

In Eq. (4), E^α and P^α are the pre-quench energy and momentum of the state $|\alpha\rangle^{\text{out}}$; $\delta(x)$ is the Dirac delta and the function F_α^Ψ is the form factor: $F_\alpha^\Psi := \langle \Omega | \Psi(0, 0) | \alpha \rangle^{\text{in}}$, calculated in the pre-quench theory. From the expansion in Eq. (4), it is straightforward to derive the post-quench evolution of a local operator Φ

$$\begin{aligned} \langle \Omega | \Phi(0, t) | \Omega \rangle &= {}_{\text{post}} \langle \Omega | \Phi(0, 0) | \Omega \rangle_{\text{post}} \\ &+ 4\pi\delta\lambda \sum_{\alpha \neq \Omega} \frac{\delta(P^\alpha)}{E^\alpha} \text{Re} \left[e^{-itE_{\text{post}}^\alpha} (F_\alpha^\Psi)^* \langle \Omega | \Phi(0, 0) | \alpha \rangle_{\text{post}}^{\text{out}} \right] \\ &+ \mathcal{O}(\delta\lambda^2), \end{aligned} \quad (5)$$

with now E_{post}^α the energy of the state $|\alpha\rangle_{\text{post}}^{\text{out}}$. At $\mathcal{O}(\delta\lambda)$, one can replace $|\alpha\rangle_{\text{post}}^{\text{out}}$ by $|\alpha\rangle^{\text{out}}$ inside the sum in Eq. (5) and, by using known properties of the form factors, is also possible to relax the ordering prescription on the momenta of the out-states [48]. We will denote then by \sum'_α , a Lorentz invariant integration over the pre-quench multiparticle states with unrestricted momenta [49]. The leading order correction to the one-point function of a local operator after a quench is therefore [35, 36]

$$\begin{aligned} \langle \Omega | \Phi(0, t) | \Omega \rangle &= {}_{\text{post}} \langle \Omega | \Phi(0, 0) | \Omega \rangle_{\text{post}} \\ &+ 4\pi\delta\lambda \sum'_{\alpha \neq \Omega} \frac{\delta(P^\alpha)}{E^\alpha} \text{Re} \left[e^{-itE_{\text{post}}^\alpha} (F_\alpha^\Psi)^* F_\alpha^\Phi \right] + \mathcal{O}(\delta\lambda^2). \end{aligned} \quad (6)$$

Consider now a semi-infinite spatial bipartition of the Hilbert space of the QFT associated to the quench problem (3). In particular, let \mathcal{L} be the semi-infinite

negative real line and \mathcal{R} the semi-infinite positive real line and denote by $\rho_{\mathcal{R}}(t) := \text{Tr}_{\mathcal{L}}[e^{-iH_{\text{post}}t}|\Omega\rangle\langle\Omega|e^{iH_{\text{post}}t}]$, the reduced density matrix after the quench obtained tracing over the left degrees of freedom. In QFT, half-space Rényi entropies after a quench $S_n(t) := \frac{1}{1-n} \log[\text{Tr}_{\mathcal{R}}\rho_{\mathcal{R}}^n(t)]$ are related to the one-point function of the twist field \mathcal{T}_n [37, 38] by

$$S_n(t) = \frac{1}{1-n} \log [\epsilon^{\Delta_{\mathcal{T}_n}} \langle\Omega|\mathcal{T}_n(0,t)|\Omega\rangle]. \quad (7)$$

In Eq. (7), ϵ is a short distance cut-off and $\Delta_{\mathcal{T}_n} = \frac{c}{12}(n - n^{-1})$ is the scaling dimension of the twist field at the QCP [50–52]. The von Neumann entropy $S(t)$ is defined through the limit $S(t) := \lim_{n \rightarrow 1} S_n(t)$.

In writing Eq. (7), a new difficulty arises: the expectation value of the twist field has to be calculated in an n -fold replicated QFT and the time evolution of the twist field after the quench is governed by the replicated Hamiltonian $\sum_{r=1}^n H_{\text{post}}^{(r)} = \sum_{r=1}^n (H^{(r)} + \delta_\lambda \int dx \Psi^{(r)})$, r being the replica index. However, when calculating the overlaps $\langle\alpha|\Omega\rangle$ at first-order in δ_λ , the sum over the replica trivializes since the perturbing field $\Psi^{(r)}$ has non-vanishing matrix elements only between particles in the same copy. One therefore gets Eq. (4) with a prefactor n in front of the sum, which only involves states within one particular replica, for instance the first. By repeating now the derivation of Eq. (6), we conclude that the leading order expansion of the twist field one-point function after a quench is

$$\begin{aligned} \langle\Omega|\mathcal{T}_n(0,t)|\Omega\rangle &= \text{post} \langle\Omega|\mathcal{T}_n(0,0)|\Omega\rangle_{\text{post}} \\ &+ 4\pi n \delta_\lambda \sum_{\substack{\alpha \neq \Omega; \\ \alpha \in \text{1st rep.}}} \frac{\delta(P^\alpha)}{E^\alpha} \text{Re} \left[e^{-itE_{\text{post}}^\alpha} (F_\alpha^\Psi)^* F_\alpha^{\mathcal{T}_n} \right] + \mathcal{O}(\delta_\lambda^2), \end{aligned} \quad (8)$$

where, as indicated, the sum only contains states in the first replica. Similarly to the discussion around Eq. (6), $F_\alpha^{\mathcal{T}_n}$ in Eq. (8) denotes the pre-quench twist-field matrix element $F_\alpha^{\mathcal{T}_n} = \langle\Omega|\mathcal{T}_n(0,0)|\alpha\rangle^{\text{in}}$.

Longitudinal Field Quench.— We examine a quench along the vertical axis of the phase diagram of the IFT depicted in Fig. 1. This quench, cf. Eq. (2), involves a sudden change of the coupling $\lambda_2 \rightarrow \lambda_2 + \delta_\lambda$ while keeping $\lambda_1 = 0$. In the lattice model described by Eq. (1), it modifies the longitudinal field $h_x \rightarrow h_x + \delta_{h_x}$ at fixed transverse field $h_z = 1$. In the presence of a longitudinal field, the Ising spin chain is strongly interacting and the perturbative approach is the only analytical device to study entanglement dynamics.

From a QFT perspective, at $\lambda_1 = 0$ and $\lambda_2 \neq 0$, both the pre- and post-quench theories are integrable. The spectrum contains of eight stable particles [42, 53], whose masses are in correspondence with the components of the Perron-Frobenius eigenvector of the Cartan matrix of the Lie algebra E_8 . We will refer to such a field theory, in

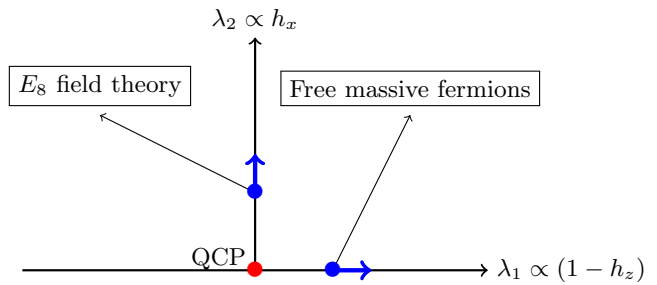


FIG. 1. Phase diagram of the IFT, described by the action (2). We consider applications of the perturbation theory to a quench of the longitudinal field $h_x \propto \lambda_2$, while keeping the transverse field $(1 - h_z) \propto \lambda_1$ at its critical value, i.e. $\lambda_1 = 0$. In the scaling limit, the pre-quench theory is integrable and corresponds to the E_8 field theory. For $\lambda_2 = 0$, the pre-quench theory can be mapped to non-interacting fermions with mass λ_1 .

short, as the E_8 field theory, see Fig. 1. The masses of the eight particles have been partially measured experimentally [54] and numerically estimated in the scaling limit using matrix product states [55]. In the E_8 field theory both the spin operator and the twist field couple to the eight one-particle states. Eqs. (6) and (8), predict in this case that at $\mathcal{O}(\delta_\lambda)$ the one-point function of the spin and the entanglement entropies must oscillate in time without relaxing. The first-order result for the order parameter [36] is re-obtained in [56]. For the time evolution of the entanglement entropies, perturbation theory, combined with Eq. (7), gives at large times

$$\begin{aligned} S_n(t) - S_n(0) &\stackrel{t \gg 1}{\geq} \frac{\delta_\lambda}{\lambda_2} \left[\frac{2n\mathcal{C}_\sigma}{1-n} \sum_{a=1}^8 \frac{\hat{F}_a^\sigma \hat{F}_a^{\mathcal{T}_n}}{r_a^2} \cos(mr_a t) \right. \\ &\quad \left. + \frac{1}{1-n} \frac{\Delta_{\mathcal{T}_n}}{2 - \Delta_\sigma} \right] + \mathcal{O}(\delta_\lambda^2). \end{aligned} \quad (9)$$

where the coefficient [63] $\mathcal{C}_\sigma = -0.065841\dots$ and the (real) normalized pre-quench one-particle form factors of the spin field [64], \hat{F}_a^σ , and the twist field [65], $\hat{F}_a^{\mathcal{T}_n}$ are also summarized in [56]. The universal ratios r_a in Eq. (9) are the masses of the particles in the E_8 field theory normalized by the mass of the lightest particle, whose value *after* the quench is m . It is finally possible [56] to extrapolate the results for the Rényi entropies to $n \rightarrow 1$, and predict the long-time limit of the von Neumann entropy. There are subleading corrections in time to Eq. (9) of order $t^{-3/2}$ (but of leading order in δ_λ) which are discussed in [56].

The field theoretical result in Eq. (9) can be tested against numerical simulations through matrix product states in the Ising spin chain near the QCP. For finding the initial state and for the time evolution we use the iTEBD algorithm [66, 67] extrapolated to the scaling limit, details are given in [56]. In a non-equilibrium protocol, the longitudinal field is quenched from h_x to

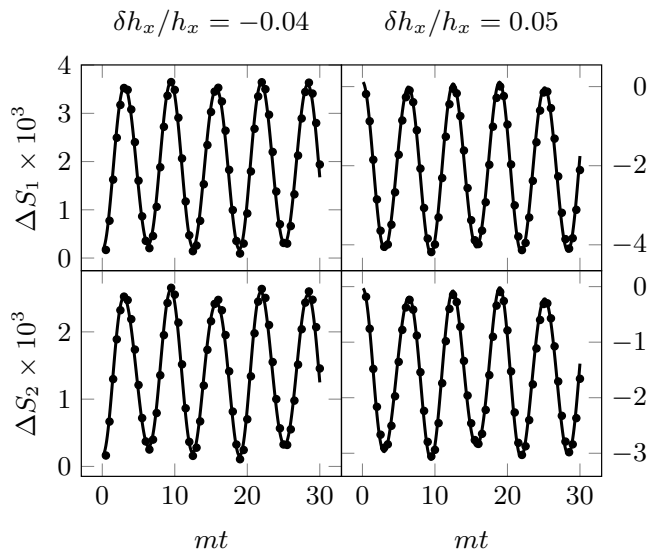


FIG. 2. The time evolution of the von Neumann entropy (top) and the second Rényi entropy (bottom) differences $\Delta S_n = S_n(t) - S_n(0)$ for quenches with $\delta h_x/h_x = -0.04$ (left) and $\delta h_x/h_x = 0.05$ (right). The dots are the extrapolated iTEBD data. Lines are the theoretical prediction from Eq. (9) ($n \rightarrow 1$ limit for von Neumann), up to the first four particles in the sum, and incorporating the two particle contributions given in [56].

$h_x + \delta h_x$ with $\delta h_x/h_x = \delta\lambda/\lambda_2 = -0.04, 0.05$. Due to the absence of visible linear growth of the entanglement entropies [56], the simulation can reach large enough time to carry out a Fourier analysis. The non-universal mass coupling relation is obtained by fitting the numerical data for the order parameter to the theoretical curve given in [56], and we have $m \approx 5.42553(h_x + \delta h_x)^{8/15}$, consistent with earlier estimates [55, 68].

According to Eq. (9), in the scaling limit, with time measured in units of m^{-1} , the time evolution of entanglement entropies should follow a universal curve. The numerical results for real time evolution in the scaling region are summarized in Fig. 2 for the von Neumann and the second Rényi entropy, showing excellent agreement with theoretical predictions obtained from Eq. (9). The curves for the entanglement entropies have been shifted vertically by an empirical value to account for higher order corrections [40] to the twist field post-quench expectation value, cf. Eq. (39) in [56]. In Fig. 3 we also show the numerical Fourier spectrum of the von Neumann entropy calculated from extrapolated data up to $mt = 170$. The Fourier transform was carried out with respect to the rescaled time mt , therefore the main frequency is at $\tilde{\omega} = 1$ for both quenches. The various peaks are related to the mass ratios of different particles summarized in [56]. For infinite time the one particle peaks would be δ -function peaks, but for finite time they have finite height. The height ratios are related to form factors of

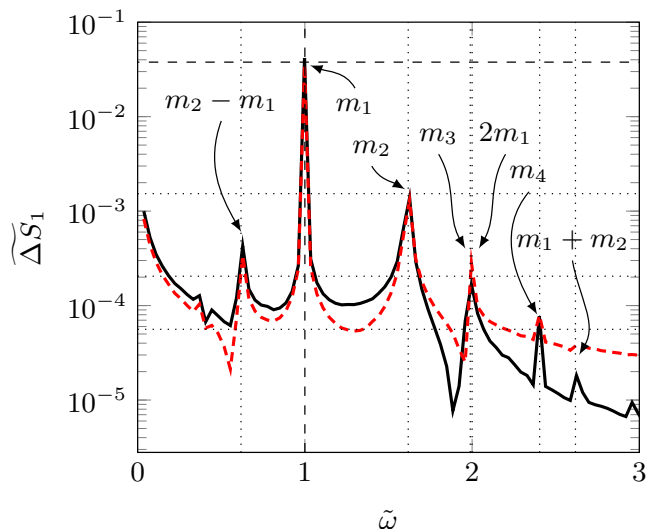


FIG. 3. Numerical Fourier transform of the variation of the von Neumann entropy (related to the variable mt) for quenches with $\delta h_x/h_x = 0.05$ (solid) and $\delta h_x/h_x = -0.04$ (dashed). Vertical lines indicate different frequencies. The horizontal lines mark the peaks corresponding to the masses of the four lightest particles. From top to bottom they correspond to m_1, m_2, m_3 and m_4 , respectively. The dashed horizontal line is set by hand, and the three dotted horizontal lines were calculated from the ratios of the one-particle form factors based on Eq. (9).

the longitudinal field and the twist fields through Eq. (9). The horizontal line in Fig. 3 related to the lightest particle is set by hand, the ones related to m_2, m_3 and m_4 are calculated from the form factors given in [56].

Transverse Field Quench.— We consider now a quench of the transverse field $h_z \rightarrow h_z + \delta h_z$ for longitudinal field $h_x = 0$. In the IFT, see Fig. 1, this protocol displaces along the horizontal axis of the phase diagram: $\lambda_1 \rightarrow \lambda_1 + \delta\lambda$, modifying the mass of the Majorana fermion [9, 69]. The ground state $|\Omega\rangle$ of the pre-quench theory can be expanded in the post-quench quasi-particle basis as

$$|\Omega\rangle = \exp \left[\int_0^\infty \frac{dp}{2\pi\tilde{e}(p)} \tilde{K}(p) a_{\text{post}}^\dagger(-p) a_{\text{post}}^\dagger(p) \right] |\Omega\rangle_{\text{post}}, \quad (10)$$

where the function $\tilde{K}(p)$ is given in [69] and $a_{\text{post}}^\dagger(p)$ are post-quench fermionic creation operators. Due to the properties of the free fermionic form factors, the expectation value of the twist field exponentiates

$$\frac{\langle \Omega | \mathcal{T}_n(0, t) | \Omega \rangle}{\text{post} \langle \Omega | \mathcal{T}_n(0, 0) | \Omega \rangle_{\text{post}}} = \exp \left[\sum_{k,l=0}^{\infty} D_{2k,2l}^c(t) \right]. \quad (11)$$

For a proof of Eq. (11), we refer to the Supplementary Material [56]. The amplitudes $D_{2k,2l}^c(t)$ contribute at leading order $\left(\frac{\delta\lambda}{\lambda_1}\right)^{k+l}$ in perturbation theory and can be systematically computed. Differently from Eq. (9),

the oscillatory first-order term is $O(t^{-3/2})$ for large time, while in [40] it was shown that $D_{2,2}^c(t) = \left(\frac{\delta_\lambda}{\lambda_1}\right)^2 [-|A|t + \mathcal{O}(1)]$. In the absence of interactions, exponentiation of second order contributions, leads then to linear growth of the Rényi entropies as a by-product of relaxation of the twist-field one-point function.

Discussion.— Absence of relaxation of the order parameter and persistent oscillations in the entanglement entropies have been observed previously in several numerical investigations of the Ising spin chain and its scaling limit [22–26]. In this Letter, we formulated a new first principle perturbative approach which quantitatively explains these phenomena. Persistent oscillations in the one-point function of a local observable are only possible if it can create a single quasi-particle excitation of the post-quench Hamiltonian. This is a necessary condition that is never satisfied in absence of interactions, as also emphasized in [35]. By mapping entanglement entropies into correlation functions of a local field, the twist field, we then provided an analogous criterion to understand when entanglement growth can slow down.

An important question is whether the exponentiation of higher orders in perturbation theory will damp the oscillatory first-order result for local observables derived in Eqs. (6) and (8). The time-scale for this to happen defines the relaxation time which is model-dependent and relates specifically to the analytic structure of the overlaps with the initial state [71, 72]. For instance, see Eq. (11), for mass quenches in free theories the relaxation time can be calculated starting from the second-order in perturbation theory. To test the robustness of the first-order result in an interacting theory, we performed in [56] additional numerical simulations. They indicate that along the E_8 line, see Fig. 1, the order parameter σ^x does not relax and the entanglement entropies still shows long-living oscillations also when the quench parameter $\delta h_x/h_x$ is of order one. Remarkably then, even after a large longitudinal field quench, the late-time dynamics continues to be qualitatively captured by first-order perturbation theory.

The formalism in this Letter allows calculating entanglement entropies in the scaling limit for any interacting massive theory without fine-tuning of the initial state. A priori this includes non-integrable models, even if the development of a perturbation series will generally be more challenging. It could be adapted to quench protocols in absence of translation invariance [73] and we believe that it will be useful for other one-dimensional systems [28, 33, 70] that show similar long-living oscillations.

Acknowledgements.— We are grateful to A. Cubero, A. Delfino and G. Takács for numerous comments on the first version of this paper. OACA and IMSZ gratefully acknowledge support from EPSRC through the standard proposal “Entanglement Measures, Twist Fields,

and Partition Functions in Quantum Field Theory” under reference number EP/P006108/1. They are also grateful to the International Institute of Physics in Natal (Brazil) for support during the workshop “Emergent Hydrodynamics in Low-Dimensional Quantum Systems” held in May 2019 during which discussions relating to this work took place. The work of IMSZ was supported by the grant “Exact Results in Gauge and String Theories” from the Knut and Alice Wallenberg foundation; JV is supported by the Brazilian Ministries MEC and MCTC and the Italian Ministry MIUR under the grant PRIN 2017 “Low-dimensional quantum systems: theory, experiments and simulations”. Part of ML’s work was carried out at the International Institute of Physics in Natal (Brazil), where his research was supported by the Brazilian Ministries MEC and MCTC. ML also acknowledges support provided from the National Research, Development and Innovation Office of Hungary, Project no. 132118 financed under the PD_19 funding scheme. We thank the High-Performance Computing Center (NPAD) at UFRN for providing computational resources.

-
- [1] J. M. Deutsch, Quantum statistical mechanics in a closed system, *Phys. Rev. A* **43**, 2046–2049 (1991).
 - [2] M. Srednicki, Chaos and quantum thermalization, *Phys. Rev. E* **50**, 888–901 (1994).
 - [3] T. Kinoshita, T. Wenger, and D. Weiss, A Quantum Newton’s Cradle, *Nature* **440**, 900 (2006).
 - [4] S. Hofferberth, I. Lesanovsky, B. Fischer, T. Schumm, and J. Schmiedmayer, Non-equilibrium coherence dynamics in one-dimensional Bose gases, *Nature* **449**, 324–327 (2007).
 - [5] M. Gring, M. Kuhnert, T. Langen, T. Kitagawa, B. Rauer, M. Schreitl, I. Mazets, D. A. Smith, E. Demler, and J. Schmiedmayer, Relaxation and Prethermalization in an Isolated Quantum System, *Science* **337**(6100), 1318–1322 (2012).
 - [6] T. Langen, S. Erne, R. Geiger, B. Rauer, T. Schweigler, M. Kuhnert, W. Rohringer, I. E. Mazets, T. Gasenzer, and J. Schmiedmayer, Experimental observation of a generalized Gibbs ensemble, *Science* **348**(6231), 207–211 (2015).
 - [7] P. Calabrese and J. L. Cardy, Evolution of entanglement entropy in one-dimensional systems, *J. Stat. Mech.* **0504**, P04010 (2005).
 - [8] P. Calabrese and J. L. Cardy, Time-dependence of correlation functions following a quantum quench, *Phys. Rev. Lett.* **96**, 136801 (2006).
 - [9] P. Calabrese, F. H. L. Essler, and M. Fagotti, Quantum Quench in the Transverse Field Ising Chain, *Phys. Rev. Lett.* **106**(22), 227203 (2011).
 - [10] M. Fagotti and F. H. L. Essler, Reduced density matrix after a quantum quench, *Phys. Rev.* **B87**, 245107 (2013).
 - [11] F. H. L. Essler and M. Fagotti, Quench dynamics and relaxation in isolated integrable quantum spin chains, *J. Stat. Mech.* **2016**(6), 064002 (2016).
 - [12] T. Mori, T. N. Ikeda, E. Kaminishi, and M. Ueda, Ther-

- malization and prethermalization in isolated quantum systems: a theoretical overview, *J. Phys.* **B51**(11), 112001 (2018).
- [13] V. Alba and P. Calabrese, Entanglement and thermodynamics after a quantum quench in integrable systems, *PNAS* **114**(30), 7947–7951 (2017).
- [14] M. Fagotti and P. Calabrese, Evolution of entanglement entropy following a quantum quench: Analytic results for the XY chain in a transverse magnetic field, *Phys. Rev.* **A78**, 010306 (2008).
- [15] A. Nahum, J. Ruhman, S. Vijay, and J. Haah, Quantum Entanglement Growth under Random Unitary Dynamics, *Phys. Rev.* **X7**, 031016 (2017).
- [16] A. Chan, A. De Luca, and J. T. Chalker, Solution of a Minimal Model for Many-Body Quantum Chaos, *Phys. Rev.* **X8**, 041019 (2018).
- [17] P. Kos, M. Ljubotina, and T. Prosen, Many-Body Quantum Chaos: Analytic Connection to Random Matrix Theory, *Phys. Rev.* **X8**, 021062 (2018).
- [18] B. Bertini, P. Kos, and T. Prosen, Entanglement Spreading in a Minimal Model of Maximal Many-Body Quantum Chaos, *Phys. Rev.* **X9**, 021033 (2019).
- [19] M. C. Bañuls, J. I. Cirac, and M. B. Hastings, Strong and Weak Thermalization of Infinite Nonintegrable Quantum Systems, *Phys. Rev. Lett.* **106**, 050405 (2011).
- [20] H. Bernien, S. Schwartz, A. Keesling, H. Levine, A. Omran, H. Pichler, S. Choi, A. S. Zibrov, M. Endres, M. Greiner, V. Vuletic, and M. Lukin, Probing many-body dynamics on a 51-atom quantum simulator, *Nature* **551** (7682) (2017).
- [21] C. Turner, A. Michailidis, D. Abanin, M. Serbyn, and Z. Papic, Weak ergodicity breaking from quantum many-body scars, *Nature Physics* **14**, 745–749 (2018).
- [22] M. Kormos, M. Collura, G. Takács, and P. Calabrese, Real time confinement following a quantum quench to a non-integrable model, *Nature Physics*. **13**, 246–249 (2017).
- [23] T. Rakovszky, M. Mestyán, M. Collura, M. Kormos, and G. Takács, Hamiltonian truncation approach to quenches in the Ising field theory, *Nucl. Phys.* **B911**, 805–845 (2016).
- [24] K. Hodsagi, M. Kormos, and G. Takacs, Quench dynamics of the Ising field theory in a magnetic field, *SciPost Phys.* **5**, 27 (2018).
- [25] A. J. A. James, R. M. Konik, and N. J. Robinson, Non-thermal States Arising from Confinement in One and Two Dimensions, *Phys. Rev. Lett.* **122**, 130603 (2019).
- [26] N. J. Robinson, A. J. A. James, and R. M. Konik, Signatures of rare states and thermalization in a theory with confinement, *Phys. Rev.* **B99**, 195108 (2019).
- [27] T. Chanda, J. Zakrzewski, M. Lewenstein, and L. Tagliacozzo, Confinement and lack of thermalization after quenches in the bosonic Schwinger model, 1909.12657 (2019).
- [28] A. Lerose, F. M. Surace, P. Mazza, G. Perfetto, M. Collura, and A. Gambassi, Quasiloclized dynamics from confinement of quantum excitations, 1911.07877 (2019).
- [29] A. Cubero and N. Robinson, Lack of thermalization in (1+1)-d QCD at large N_c , arXiv:1908.00270 (2020).
- [30] G. Magnifico, M. Dalmonte, P. Facchi, S. Pascazio, F. Pepe, and E. Ercolessi, Real Time Dynamics and Confinement in the \mathbb{Z}_n Schwinger-Weyl lattice model for 1+1 QED, arXiv:1909.04821 (2019).
- [31] S. Pai and M. Pretko, Fractons from confinement, 1909.12306 (2019).
- [32] M. Medenjak, B. Buca, and D. Jaksch, The isolated Heisenberg magnet as a quantum time crystal, arXiv:1905.08266 (2019).
- [33] F. Liu, R. Lundgren, P. Titum, G. Pagano, J. Zhang, C. Monroe, and A. V. Gorshkov, Confined Quasiparticle Dynamics in Long-Range Interacting Quantum Spin Chains, *Phys. Rev. Lett.* **122**, 150601 (2019).
- [34] V. Korepin, N. Bogoliugov, and A. Izergin, Quantum inverse scattering method and correlation functions, Cambridge University Press, Cambridge (1993).
- [35] G. Delfino, Quantum quenches with integrable pre-quench dynamics, *J. Phys.* **A47**(40), 402001 (2014).
- [36] G. Delfino and J. Viti, On the theory of quantum quenches in near-critical systems, *J. Phys.* **A50**(8), 084004 (2017).
- [37] P. Calabrese and J. L. Cardy, Entanglement entropy and quantum field theory, *J. Stat. Mech.* **0406**, P002 (2004).
- [38] J. L. Cardy, O. A. Castro-Alvaredo, and B. Doyon, Form factors of branch-point twist fields in quantum integrable models and entanglement entropy, *J. Stat. Phys.* **130**, 129–168 (2008).
- [39] O. A. Castro-Alvaredo and B. Doyon, Bi-partite entanglement entropy in massive 1+1-dimensional quantum field theories, *J. Phys.* **A42**, 504006 (2009).
- [40] O. A. Castro-Alvaredo, M. Lencsés, I. M. Szécsényi, and J. Viti, Entanglement Dynamics after a Quench in Ising Field Theory: A Branch Point Twist Field Approach, *JHEP* **2019**, 79 (2019).
- [41] A. A. Belavin, A. M. Polyakov, and A. B. Zamolodchikov, Infinite Conformal Symmetry in Two-Dimensional Quantum Field Theory, *Nucl. Phys.* **B241**, 333–380 (1984).
- [42] A. B. Zamolodchikov, Integrals of Motion and S Matrix of the (Scaled) $T = T_c$ Ising Model with Magnetic Field, *Int. J. Mod. Phys.* **A4**, 4235 (1989).
- [43] G. Delfino, Integrable field theory and critical phenomena: The Ising model in a magnetic field, *J. Phys.* **A37**, R45 (2004).
- [44] G. Mussardo, *Statistical Field Theory: An introduction to exactly solved models in Statistical Physics* (Second Ed.), OUP (2020).
- [45] G. Delfino, G. Mussardo, and P. Simonetti, Nonintegrable quantum field theories as perturbations of certain integrable models, *Nucl. Phys.* **B473**, 469–508 (1996).
- [46] K. Hodsagi, M. Kormos, and G. Takacs, Perturbative post-quench overlaps in quantum field theory, *JHEP* **2019** (2019).
- [47] If $|p_1, \dots, p_n\rangle_{\text{post}}^{\text{out}}$ is a n -particle out state of H_{post} , the Lorentz invariant integration measure in 1+1 dimensions is $\sum_{\alpha} := \sum_{n=0}^{\infty} \int_{p_1 < p_2 < \dots < p_n} \prod_{j=1}^n \frac{dp_j}{2\pi\epsilon(p_j)}$.
- [48] F. Smirnov, Form factors in completely integrable models of quantum field theory, *Adv. Series in Math. Phys.* **14**, World Scientific, Singapore (1992).
- [49] If $|p_1, \dots, p_n\rangle$ is a n -particle eigenstate of the pre-quench Hamiltonian H , the symmetrized Lorentz invariant integration measure in the text is $\sum'_{\alpha} := \sum_{n=0}^{\infty} \frac{1}{n!} \int_{\mathbb{R}^n} \prod_{j=1}^n \frac{dp_j}{2\pi\epsilon(p_j)}$.
- [50] L. Dixon, D. Friedan, E. Martinec, and S. Shenker, The conformal field theory of orbifolds, *Nucl. Phys.* **B282**, 13–73 (1987).
- [51] P. Bouwknegt, Coset construction for winding subalgebras and applications, q-alg/9610013 .
- [52] L. Borisov, M. B. Halpern, and C. Schweigert, Systematic

- approach to cyclic orbifolds, *Int. J. Mod. Phys. A* **13**, 125–168 (1998).
- [53] A. B. Zamolodchikov, Integrable field theory from conformal field theory, *Adv. Stud. Pure Math.* **19**, 641–674 (1989).
- [54] R. Coldea, D. A. Tennant, E. M. Wheeler, E. Wawrzynska, D. Prabhakaran, M. Telling, K. Habicht, P. Smeibidl, and K. Kiefer, Quantum Criticality in an Ising Chain: Experimental Evidence for Emergent E_8 Symmetry, *Science* **327**(5962), 177–180 (2010).
- [55] J. A. Kjäll, F. Pollmann, and J. E. Moore, Bound states and E_8 symmetry effects in perturbed quantum Ising chains, *Phys. Rev.* **B83**, 020407 (2011).
- [56] See Supplemental Material [url] for details about the analytic calculation of the entropies and the numerical study in the scaling limit. The Supplemental Material also includes Refs. [57–62] below.
- [57] V. Fateev, The exact relations between the coupling constants and the masses of particles for the integrable perturbed conformal field theories, *Phys. Lett.* **B324**(1), 45–51 (1994).
- [58] G. Delfino and P. Simonetti, Correlation functions in the two-dimensional Ising model in a magnetic field at $T = T_c$, *Phys. Lett.* **B383**, 450–456 (1996).
- [59] F. Pollmann, Efficient Numerical Simulations Using Matrix-Product States, 2016.
- [60] E. Forest and R. D. Ruth, Fourth-order symplectic integration, *Physica* **43D**(1), 105 – 117 (1990).
- [61] P. Calabrese, J. Cardy, and I. Peschel, Corrections to scaling for block entanglement in massive spin-chains, *J. Stat. Mech.* **1009**, P09003 (2010).
- [62] J. Cardy and P. Calabrese, Unusual corrections to scaling in entanglement entropy, *J. Stat. Mech.* **2010**(4), 04023 (2010).
- [63] V. Fateev, S. L. Lukyanov, A. B. Zamolodchikov, and A. B. Zamolodchikov, Expectation values of local fields in Bullough-Dodd model and integrable perturbed conformal field theories, *Nucl. Phys.* **B516**, 652–674 (1998).
- [64] G. Delfino and G. Mussardo, The Spin spin correlation function in the two-dimensional Ising model in a magnetic field at $T = T_c$, *Nucl. Phys.* **B455**, 724–758 (1995).
- [65] O. A. Castro-Alvaredo, Massive Corrections to Entanglement in Minimal E_8 Toda Field Theory, *SciPost Phys.* **2**(1), 008 (2017).
- [66] G. Vidal, Efficient Simulation of One-Dimensional Quantum Many-Body Systems, *Phys. Rev. Lett.* **93**, 040502 (2004).
- [67] G. Vidal, Classical Simulation of Infinite-Size Quantum Lattice Systems in One Spatial Dimension, *Phys. Rev. Lett.* **98**, 070201 (2007).
- [68] M. Henkel and H. Saleur, The two-dimensional Ising model in the magnetic field: a numerical check of Zamolodchikov conjecture, *J. Phys.* **A22**(11), L513–L518 (1989).
- [69] D. Schuricht and F. H. L. Essler, Dynamics in the Ising field theory after a quantum quench, *J. Stat. Mech.* **1204**, P04017 (2012).
- [70] C.-J. Lin and O. I. Motrunich, Quasiparticle explanation of the weak-thermalization regime under quench in a nonintegrable quantum spin chain, *Phys. Rev.* **A95**, 023621 (2017).
- [71] A. Cubero and D. Schuricht, Quantum quench in the attractive regime of the sine-Gordon model, *J. Stat. Mech.* **103106** (2017).
- [72] D. Horvath, M. Kormos, and G. Takacs, Overlap singularity and time evolution in integrable quantum field theory, *JHEP* **2018** (2018).
- [73] G. Delfino, Persistent oscillations after quantum quenches, *Nucl. Phys.* **B954** (2020) 115002.

SUPPLEMENTARY MATERIAL

The Supplementary Material is organized as follows. In Section 1 we summarize the main analytical results that we have used in our Letter, particularly when comparing the predictions of quench perturbation theory [1, 2] to lattice numerical calculations in the scaling limit. These analytical results are principally the form factors of local fields in the theories under consideration. The fields involved here are the branch point twist field whose correlators are directly linked to measures of entanglement, and the field associated with the coupling whose sudden change generates the quench.

In our Letter we have mainly discussed the longitudinal field quench (for critical transverse field). In the QFT setting, this is equivalent to a mass quench in the E_8 minimal Toda field theory. The mass $m_{0,1}$ of the lightest particle in the model before the quench (see Section 1) and the coupling constant λ_2 are related as

$$m_{0,1} = \kappa \lambda_2^{\frac{8}{15}}, \quad \text{with} \quad \kappa = 4.40490858\dots, \quad (1)$$

where the constant κ has an analytical expression in terms of Γ -functions first found in [3]. Therefore a change of the longitudinal field h_x proportional to λ_2 is equivalent to a change of the masses of the eight particles in the spectrum, which are all multiples of $m_{0,1}$. As shown in Fig. 1 and equation (2) of the Letter, in the QFT, the perturbing field is the spin field $\sigma(x, t)$. We analyze such a quench in Section 1 of the supplementary material.

In Section 2, we also present a complete proof of the exponentiation of the one-point function of the branch point twist field in the case of a transverse field quench (for zero longitudinal field). That is equivalent to a mass quench in Ising field theory since now the fermion mass m_0 is proportional to $|h_z - 1|$, where h_z is the transverse field. Our proof complements the detailed study presented in [4]. In this case the perturbing field is the energy field $\varepsilon(x, t)$ as also shown in Fig. 1 of the Letter.

In Section 3 we provide a description of the numerical techniques, with additional results not included in the Letter. Finally in Section 4 we comment on the robustness of entanglement oscillations at higher order in perturbation theory.

1 Longitudinal Field Quench: Mass Quench in E_8 Minimal Toda Field Theory

Let us start by fixing the basic definitions and notations for the form factors that we have employed in the present work. Although in our Letter we have written formulae involving form factors of an arbitrary state $|\alpha\rangle^{\text{out/in}}$, in practise the only form factors that have been analytically evaluated are those associated with one- and two-particle states. We will therefore only review those here. In a 1+1-dimensional QFT we define the one- and the two-particle form factors of a local, spinless field \mathcal{O} as the matrix elements

$$F_{a_1}^{\mathcal{O}} := \langle \Omega | \mathcal{O}(0, 0) | \theta_1 \rangle_{a_1} \quad \text{and} \quad F_{a_1 a_2}^{\mathcal{O}}(\theta_1 - \theta_2) := \langle \Omega | \mathcal{O}(0, 0) | \theta_1 \theta_2 \rangle_{a_1 a_2}, \quad (2)$$

where a_1, a_2 are particle quantum numbers, θ_1, θ_2 are rapidities, in terms of which—and with a slight abuse of notations—the energy and momentum are given by $e_a(\theta) = m_{0,a} \cosh \theta$ and $p_a(\theta) = m_{0,a} \sinh \theta$, where $m_{0,a}$ is the mass of a particle of type a in the pre-quench theory. The state $|\Omega\rangle$ is the pre-quench vacuum.

n	2	3	4
$\hat{F}_1^{\mathcal{T}_n}$	-0.17124900374494678	-0.1996259878353373	-0.20930848250173
$\hat{F}_2^{\mathcal{T}_n}$	0.07005900535572894	0.08788104227633028	0.094313951168679
$\hat{F}_3^{\mathcal{T}_n}$	-0.03440203483936546	-0.04473113820315836	-0.048562882373633
$\hat{F}_4^{\mathcal{T}_n}$	0.023657419055677746	0.031870010789866426	0.0349996171170825

Table 1: Newly evaluated (normalized) one-particle form factors of the branch point twist field for the four lightest particles in the spectrum. The hat in $\hat{F}_i^{\mathcal{T}_n}$ indicates normalization by the vacuum expectation value of the branch point twist field.

In general, $|\theta_1 \dots \theta_k\rangle_{a_1 \dots a_k}$, is an asymptotic *in*-state of k particles and $|\Omega\rangle$ is the ground state. For spinless fields in relativistic QFT the one-particle form factors are rapidity-independent whereas the two-particle form factors depend only upon rapidity differences, hence our notation. It is also useful to introduce the normalized one-particle form factor as

$$\hat{F}_{a_1}^{\mathcal{O}} := \frac{\langle \Omega | \mathcal{O}(0,0) | \theta_1 \rangle_{a_1}}{\langle \Omega | \mathcal{O}(0,0) | \Omega \rangle}, \quad (3)$$

for the spin field and the twist field we will use the shorthand notation $\langle \Omega | \sigma(0,0) | \Omega \rangle \equiv \bar{\sigma}$ and $\langle \Omega | \mathcal{T}_n(0,0) | \Omega \rangle \equiv \tau_n$.

The E_8 minimal Toda field theory is an integrable model with diagonal scattering matrix and an eight particle spectrum. They were both first given in the seminal papers [5, 6]. The mass spectrum takes the form

$$r_2 = 2 \cos \frac{\pi}{5}, \quad r_3 = 2 \cos \frac{\pi}{30}, \quad r_4 = 2r_2 \cos \frac{7\pi}{30}, \quad r_5 = 2r_2 \cos \frac{2\pi}{15},$$

$$r_6 = r_2 r_3, \quad r_7 = r_2 r_4, \quad r_8 = r_2 r_5, \quad (4)$$

where $r_i := m_{0,i}/m_{0,1}$ (hence, $r_1 = 1$). It should be noticed that the ratios r_i are the same for both the pre-quench and post-quench theories as a consequence of universality of the scaling limit.

1.1 One-Particle Form Factors

As we have seen in equation (9) of the Letter the calculation of the entanglement entropies is based upon the knowledge of the one-particle form factors of the branch point twist field and the spin field. So far the only computation of the twist field form factors in this theory was performed in [7]. There, explicit values of the form factors of the first four lightest particles for $n = 2$ were given, whereas for $2 < n \leq 4$ the values of $\hat{F}_a^{\mathcal{T}_n}$ were presented graphically. However, while carrying out detailed comparison with the lattice results in the scaling limit, we realized that it was critical to have a more accurate evaluation of the quantities $\hat{F}_a^{\mathcal{T}_n}$ with $n = 2, 3, 4$. The values given in [7] were dependent on the asymptotic behaviour of certain two-particle form factors, and we have realized that this asymptotic value was systematically underestimated in [7]. In Table 1 we present the values of $\hat{F}_a^{\mathcal{T}_n}$ with $n = 2, 3, 4$ as newly obtained using a different technique (we will present further details in subsection 1.2). For $n = 2$ they differ from those presented in [7] by between 10% and 20% (depending on the particle). This has allowed us to reach a much improved matching with numerical values.

As we can see, equation (9) in the Letter also requires the knowledge of one-particle form factors of the spin field. These were computed in [8, 9]. Their (normalized) values are given in Table 2.

\hat{F}_1^σ	\hat{F}_2^σ	\hat{F}_3^σ	\hat{F}_4^σ
-0.64090211	0.33867436	-0.18662854	0.14277176
\hat{F}_5^σ	\hat{F}_6^σ	\hat{F}_7^σ	\hat{F}_8^σ
0.06032607	-0.04338937	0.01642569	-0.00303607

Table 2: Normalized one-particle form factors of the spin field $\hat{F}_i^\sigma = F_i^\sigma/\bar{\sigma}$, where $\bar{\sigma}$ is the expectation value of the spin field.

In order to compute the von Neumann entropy we also need the values of

$$g_a := \lim_{n \rightarrow 1} \frac{\hat{F}_a^{\mathcal{T}_n}}{1-n}. \quad (5)$$

It is well-known that the functions $\hat{F}_a^{\mathcal{T}_n}$ tend to zero for $n \rightarrow 1$. However, the precise asymptotics was not investigated in [7]. This asymptotics can be studied by analysing the consistency equations that these form factors must satisfy and which were given in [7]. These give rise to a Taylor expansion in powers of $n - 1$, starting with power one. Once more, the derivation relies heavily on properties of the functions that enter the two particle form factors. We will briefly discuss these below. Table 3 gives the values of the first four functions g_a .

1.2 Two-Particle Form Factors

In [7] the two-particle form factors $F_{11}^{\mathcal{T}_n}(\theta)$ and $F_{12}^{\mathcal{T}_n}(\theta)$ were also computed. Here we are referring always to particles in the same copy so we omit copy numbers. They are given by

$$F_{11}^{\mathcal{T}_n}(\theta) = \frac{\tau_n Q_{11}^{\mathcal{T}_n}(\theta)}{2n K_{11}(\theta; n)} \prod_{\alpha=\frac{2}{3}, \frac{2}{5}, \frac{1}{15}} B_\alpha(\theta; n) \frac{f_{11}(\theta; n)}{f_{11}(i\pi; n)}, \quad (6)$$

and

$$F_{12}^{\mathcal{T}_n}(\theta) = \frac{\tau_n Q_{12}^{\mathcal{T}_n}(\theta)}{2n} \prod_{\alpha=\frac{4}{5}, \frac{3}{5}, \frac{7}{15}, \frac{4}{15}} B_\alpha(\theta; n) \frac{f_{12}(\theta; n)}{f_{12}(i\pi; n)}, \quad (7)$$

g_1	-0.4971505471133315
g_2	0.10034674000675149
g_3	-0.03659195487267996
g_4	0.01914945194919403

Table 3: The functions (5) for the four lightest particles in the spectrum.

with

$$f_{11}(\theta; n) = -i \sinh \frac{\theta}{2n} \exp \left[2 \int_0^\infty \frac{dt}{t} \frac{\cosh \frac{t}{10} + \cosh \frac{t}{6} + \cosh \frac{13t}{30}}{\cosh \frac{t}{2} \sinh(nt)} \sin^2 \left(\frac{it}{2} \left(n + \frac{i\theta}{\pi} \right) \right) \right], \quad (8)$$

and

$$f_{12}(\theta; n) = \exp \left[2 \int_0^\infty \frac{dt}{t} \frac{\cosh \frac{t}{10} + \cosh \frac{3t}{10} + \cosh \frac{t}{30} + \cosh \frac{7t}{30}}{\cosh \frac{t}{2} \sinh(nt)} \sin^2 \left(\frac{it}{2} \left(n + \frac{i\theta}{\pi} \right) \right) \right], \quad (9)$$

where

$$K_{11}(\theta; n) = \frac{\sinh \left(\frac{i\pi - \theta}{2n} \right) \sinh \left(\frac{i\pi + \theta}{2n} \right)}{\sin \frac{\pi}{n}}, \quad (10)$$

$$B_\alpha(\theta; n) = \sinh \left(\frac{i\pi\alpha - \theta}{2n} \right) \sinh \left(\frac{i\pi\alpha + \theta}{2n} \right), \quad (11)$$

τ_n is the vacuum expectation value of the branch point twist field and the functions $Q_{ij}^{\mathcal{T}_n}(\theta)$ have the general structure

$$Q_{11}^{\mathcal{T}_n}(\theta) = A_{11}(n) + B_{11}(n) \cosh \frac{\theta}{n} + C_{11}(n) \cosh^2 \frac{\theta}{n}, \quad (12)$$

and

$$Q_{12}^{\mathcal{T}_n}(\theta) = A_{12}(n) + B_{12}(n) \cosh \frac{\theta}{n} + C_{12}(n) \cosh^2 \frac{\theta}{n}, \quad (13)$$

with coefficients that can be determined for each value of n . They have also been re-evaluated with greater precision for this work and are listed in Table 4.

n	2	3	4
$A_{11}(n)$	0.05028656966443226	0.008222663493673649	0.003094920413703075
$B_{11}(n)$	0.0011995725313121055	-0.005436476679120888	-0.004685055209534106
$C_{11}(n)$	0.009415788449439522	0.0053536637424471565	0.0032612776790863058
$A_{12}(n)$	-0.03893395394244009	-0.0052884492808026595	-0.0014212064608825764
$B_{12}(n)$	-0.0006333785909299339	0.0024712680272948595	0.0017331405976600545
$C_{12}(n)$	-0.004484918093780377	-0.002327262587055512	-0.0011767365122042212

Table 4: The coefficients of the functions $Q_{11}^{\mathcal{T}_n}(\theta)$ and $Q_{12}^{\mathcal{T}_n}(\theta)$.

At the heart of these improved values is the improved evaluation of the the leading asymptotics of the functions $f_{11}(\theta, n)$, $f_{12}(\theta, n)$ for $\theta \rightarrow \infty$. The understanding of this asymptotic plays an important role in fixing the one-particle form factors because the two-particle form factors are expected to satisfy the clustering property in momentum space, namely

$$\lim_{\theta \rightarrow \infty} F_{a_1 a_2}^{\mathcal{T}_n}(\theta) \propto F_{a_1}^{\mathcal{T}_n} F_{a_2}^{\mathcal{T}_n}. \quad (14)$$

For $a_1 = a_2 = 1$ and $a_1 = 1, a_2 = 2$ this gives two of the conditions that were employed in [7] to fix the one-particle form factors. It turns out that both functions $f_{11}(\theta, n)$ and $f_{12}(\theta, n)$ can be expressed as products of the following blocks:

$$f(\theta, \alpha; n) = \exp \left\{ 2 \int_0^\infty \frac{dt}{t} \frac{\cosh \left[t \left(\alpha - \frac{1}{2} \right) \right]}{\cosh \left(\frac{t}{2} \right)} \frac{\sin^2 \left(\frac{t[i\pi n - \theta]}{2\pi} \right)}{\sinh(nt)} \right\}, \quad (15)$$

for particular choices of α . In fact

$$f_{11}(\theta, n) = f(\theta, 0; n) f(\theta, \frac{2}{3}; n) f(\theta, \frac{2}{5}; n) f(\theta, \frac{1}{15}; n), \quad (16)$$

$$f_{12}(\theta, n) = f(\theta, \frac{4}{5}; n) f(\theta, \frac{3}{5}; n) f(\theta, \frac{7}{15}; n) f(\theta, \frac{4}{15}; n). \quad (17)$$

A natural simplification of the formula (15) that helps to extract the asymptotics is to pull out a factor $f_0(\theta, n) := f(\theta, 0; n)$ using the integral representation

$$\begin{aligned} f(\theta, \alpha; n) &= f_0(\theta; n) \exp \left\{ 2 \int_0^\infty \frac{dt}{t} \left[\frac{\cosh \left[t \left(\alpha - \frac{1}{2} \right) \right]}{\cosh \left(\frac{t}{2} \right)} - 1 \right] \frac{\sin^2 \left(\frac{t[i\pi n - \theta]}{2\pi} \right)}{\sinh(nt)} \right\} \\ &= f_0(\theta; n) \exp \left\{ -4 \int_0^\infty \frac{dt}{t} \frac{\sinh \left(\frac{t}{2} \alpha \right) \sinh \left(\frac{t}{2} (1 - \alpha) \right)}{\cosh \left(\frac{t}{2} \right)} \frac{\sin^2 \left(\frac{t[i\pi n - \theta]}{2\pi} \right)}{\sinh(nt)} \right\} \\ &= f_0(\theta; n) \mathcal{N}(\alpha; n) \exp \left\{ 2 \int_0^\infty \frac{dt}{t} \frac{\sinh \left(\frac{t}{2} \alpha \right) \sinh \left(\frac{t}{2} (1 - \alpha) \right) \cos \left(\frac{t[i\pi n - \theta]}{\pi} \right)}{\cosh \left(\frac{t}{2} \right) \sinh(nt)} \right\}, \end{aligned} \quad (18)$$

with

$$\mathcal{N}(\alpha; n) = \exp \left\{ -2 \int_0^\infty \frac{dt}{t} \frac{\sinh \left(\frac{t}{2} \alpha \right) \sinh \left(\frac{t}{2} (1 - \alpha) \right)}{\cosh \left(\frac{t}{2} \right) \sinh(nt)} \right\}. \quad (19)$$

For large θ , one can then show that

$$\lim_{\theta \rightarrow \infty} f(\theta, \alpha; n) = \mathcal{N}(\alpha; n) \lim_{\theta \rightarrow \infty} f_0(\theta; n) \sim \frac{\mathcal{N}(\alpha; n)}{2i} e^{\frac{\theta}{2n}}. \quad (20)$$

It is easy to show that $\mathcal{N}(\alpha; n)$ are convergent integrals, but the remaining integral

$$\begin{aligned} \tilde{I}(\theta, \alpha; n) &= 2 \int_0^\infty \frac{dt}{t} \frac{\sinh \left(\frac{t}{2} \alpha \right) \sinh \left(\frac{t}{2} (1 - \alpha) \right) \cos \left(\frac{t[i\pi n - \theta]}{\pi} \right)}{\cosh \left(\frac{t}{2} \right) \sinh(nt)} \\ &= 4 \int_0^\infty \frac{dt}{t} \frac{\sinh \left(\frac{t}{2} \alpha \right) \sinh \left(\frac{t}{2} (1 - \alpha) \right) \sinh \left(\frac{t}{2} \right) \cos \left(\frac{t[i\pi n - \theta]}{\pi} \right)}{\sinh(t) \sinh(nt)}, \end{aligned} \quad (21)$$

needs regularization. Our strategy is to express the $\sinh t$ in the denominator as

$$\frac{1}{\sinh t} = 2 \sum_{k=0}^{N-1} e^{-(2k+1)t} + \frac{e^{-2Nt}}{\sinh t}, \quad (22)$$

and use the integral identity

$$\begin{aligned} \int_0^\infty \frac{dt \sinh(\beta t) \sinh(\gamma t) e^{-\mu t}}{t \sinh(\delta t)} &= \frac{1}{2} \log \omega(\beta, \gamma, \mu, \delta) \\ &= \frac{1}{2} \log \left\{ \frac{\Gamma\left(\frac{\beta+\gamma+\mu+\delta}{2\delta}\right) \Gamma\left(\frac{-\beta-\gamma+\mu+\delta}{2\delta}\right)}{\Gamma\left(\frac{-\beta+\gamma+\mu+\delta}{2\delta}\right) \Gamma\left(\frac{\beta-\gamma+\mu+\delta}{2\delta}\right)} \right\}. \end{aligned} \quad (23)$$

The regularized integral then is

$$\begin{aligned} \tilde{I}(\theta, \alpha, N; n) &= 2 \int_0^\infty \frac{dt \sinh\left(\frac{t}{2}\alpha\right) \sinh\left(\frac{t}{2}(1-\alpha)\right) \cos\left(\frac{t[i\pi n - \theta]}{\pi}\right)}{t \cosh\left(\frac{t}{2}\right) \sinh(nt)} e^{-2Nt} \\ &+ \sum_{k=0}^{N-1} \log \frac{\omega\left(\frac{\alpha}{2}, \frac{1-\alpha}{2}, 2k + \frac{1}{2} + n + i\frac{\theta}{\pi}, n\right) \omega\left(\frac{\alpha}{2}, \frac{1-\alpha}{2}, 2k + \frac{1}{2} - n - i\frac{\theta}{\pi}, n\right)}{\omega\left(\frac{\alpha}{2}, \frac{1-\alpha}{2}, 2k + \frac{3}{2} + n + i\frac{\theta}{\pi}, n\right) \omega\left(\frac{\alpha}{2}, \frac{1-\alpha}{2}, 2k + \frac{3}{2} - n - i\frac{\theta}{\pi}, n\right)}. \end{aligned} \quad (24)$$

The asymptotics of the Γ function for large imaginary values is

$$\lim_{y \rightarrow \infty} \Gamma(x + iy) \sim \sqrt{2\pi} y^{x-1/2+iy} e^{-i\pi/4+i\pi x/2-iy-\pi y/2+\mathcal{O}(1/y)}, \quad (25)$$

hence

$$\lim_{\theta \rightarrow \infty} \omega(\beta, \gamma, \mu + i\theta/\pi, n) = 1. \quad (26)$$

Since the value of $\tilde{I}(\theta, \alpha, N; n)$ is independent of the value of N

$$\lim_{\theta \rightarrow \infty} \tilde{I}(\theta, \alpha, N; n) = \lim_{\theta \rightarrow \infty} \tilde{I}(\theta, \alpha, \infty; n) = 0, \quad (27)$$

which then gives the behaviour (20).

With the more accurate evaluation of the asymptotics, the solution of the consistency equations for the first four one-particle and first two two-particle form factors boils down of solving a cubic equation, whose appropriate solution is chosen by the property that it should vanish as n approaches 1. The expressions for the coefficients are cumbersome, hence we do not list them over here, only the numerical values for $n = 2, 3, 4$ in Table 1 and Table 4.

In order to evaluate the von Neumann entropy we also need the asymptotic values of the constants in equations (12) and (13) as $n \rightarrow 1$. This requires the values

$$\lim_{n \rightarrow 1} (1-n)K_{11}(\theta; n) = \pi \cosh^2 \frac{\theta}{2}, \quad (28)$$

and

$$B_\alpha(\theta; 1) = \frac{1}{2}(\cos(\alpha\pi) - \cosh \theta), \quad (29)$$

and the fact that the functions $f(\theta, \alpha; n)$ all have leading behaviour $\mathcal{O}((n-1)^0)$ as n tends to 1. Employing once more the improved asymptotics we have obtained the results of Table 3 and Table 5. It is important to note, that it was crucial to have an explicit solution for the coefficients to extract the $n \rightarrow 1$ limit, since the fit from different values of $1 < n < 2$ can give misleading coefficients in certain cases.

We point out, that to evaluate integrals of the two-particle form factors, like in Eq. (34), in a numerically stable way, we need to regularize the integrals in (15) on the line as was presented

$A_{11}(n)$	$0.2036599645689198 + \mathcal{O}(n-1)$
$B_{11}(n)$	$0.0418206628975086 + \mathcal{O}(n-1)$
$C_{11}(n)$	$\mathcal{O}(n-1)$
$A_{12}(n)$	$-0.4583212393562862(n-1) + \mathcal{O}((n-1)^2)$
$B_{12}(n)$	$-0.0581657847796917(n-1) + \mathcal{O}((n-1)^2)$
$C_{12}(n)$	$\mathcal{O}((n-1)^2)$

Table 5: $n \rightarrow 1$ leading behaviour of the coefficients of (12) and (13). Note that the precise coefficient of $(n-1)$ in $C_{11}(n)$ is not given because such term will give no overall contribution to the von Neumann entropy. The same applies to $C_{12}(n)$.

above for $\tilde{I}(\theta, \alpha; n)$, instead of using the formula where the $f_0(\theta, 0; n)$ factor was pulled out of the expression. The reason is that $\tilde{I}(\theta, \alpha; n)$ diverges around $\theta = 0$, which is compensated by the $f_0(\theta, 0; n)$ term leading to a finite result, however this makes the numerical evaluation unstable around $\theta = 0$.

For the spin field, the structure of the two-particle form factors is very similar to that of the twist field form factors but slightly simpler. The formulae for $F_{a_1 a_2}^\sigma(\theta)$ were all given in [8, 9]. Here we will only recall

$$F_{11}^\sigma(\theta) = \frac{\bar{\sigma} \cos^2 \frac{\pi}{3} \cos^2 \frac{\pi}{5} \cos^2 \frac{\pi}{30} Q_{11}^\sigma(\theta)}{\prod_{\alpha=\frac{2}{3}, \frac{2}{5}, \frac{1}{15}} B_\alpha(\theta; 1)} \frac{f_{11}(\theta; 1)}{f_{11}(i\pi; 1)}, \quad (30)$$

and

$$F_{12}^\sigma(\theta) = \frac{\bar{\sigma} \cos^2 \frac{3\pi}{10} \cos^2 \frac{2\pi}{5} \cos^2 \frac{7\pi}{30} \cos^2 \frac{2\pi}{15} Q_{12}^\sigma(\theta)}{\prod_{\alpha=\frac{4}{5}, \frac{3}{5}, \frac{7}{15}, \frac{4}{15}} B_\alpha(\theta; 1)} \frac{f_{12}(\theta; 1)}{f_{12}(i\pi; 1)}. \quad (31)$$

In [9] functions

$$Q_{11}^\sigma(\theta) = c_{11}^1 \cosh \theta + c_{11}^0, \quad Q_{12}^\sigma(\theta) = c_{12}^2 \cosh^2 \theta + c_{12}^1 \cosh \theta + c_{12}^0, \quad (32)$$

were computed and the coefficients are

$$\begin{aligned} c_{11}^1 &= -2.093102832, & c_{11}^0 &= -10.19307727, & c_{12}^2 &= -7.979022182, \\ c_{12}^1 &= -71.79206351, & \text{and} & & c_{12}^0 &= -70.29218939. \end{aligned} \quad (33)$$

1.3 Entanglement Dynamics after a Quench of the Longitudinal Field

Following Eq. (9) of the Letter and the formulae given in [1, 4] we have that the change experienced by the one-point function of the branch point twist field after a quench of the longitudinal field takes the form

$$\begin{aligned} \langle \Omega | \mathcal{T}_n(0, t) | \Omega \rangle &= \text{post} \langle \Omega | \mathcal{T}_n(0, 0) | \Omega \rangle_{\text{post}} + \delta_\lambda n \sum_{a=1}^8 \frac{2}{m_{0,a}^2} F_a^\sigma F_a^{\mathcal{T}_n} \cos(m_a t) \\ &+ 2\delta_\lambda n \sum_{a,b=1}^8 \int_{-\infty}^{\infty} \frac{dp_a dp_b}{2\pi e_a e_b} \frac{\delta(p_a + p_b)}{e_a + e_b} \text{Re} \left[[F_{ab}^\sigma(p_a, p_b)]^* F_{ab}^{\mathcal{T}_n}(p_a, p_b) [e^{-i(\tilde{e}_a + \tilde{e}_b)t}] \right] + \mathcal{O}(\delta_\lambda^2), \end{aligned} \quad (34)$$

where δ_λ is the small change of the QFT coupling constant $\lambda_2 \propto h_x$. Here we also used the fact that the one particle form factors are real. We also remind that $\tilde{e}_a(p) = \sqrt{m_a^2 + p^2}$, being m_a the post-quench mass of the type- a particle.

From this expression it is relatively straightforward to arrive at the formula for the change of the entanglement entropies given in the Letter, see Eq. (9) there. We know from the definition that

$$S_n(t) := \frac{1}{1-n} \log \left(\epsilon^{\Delta\tau_n} \langle \Omega | \mathcal{T}_n(0, t) | \Omega \rangle \right), \quad (35)$$

therefore

$$\begin{aligned} S_n(t) - S_n(0) &:= \frac{1}{1-n} \log \left(\frac{\langle \Omega | \mathcal{T}_n(0, t) | \Omega \rangle}{\langle \Omega | \mathcal{T}_n(0, 0) | \Omega \rangle} \right) \\ &= \frac{1}{1-n} \log \left(1 + \frac{\langle \Omega | \mathcal{T}_n(0, t) | \Omega \rangle - \langle \Omega | \mathcal{T}_n(0, 0) | \Omega \rangle}{\langle \Omega | \mathcal{T}_n(0, 0) | \Omega \rangle} \right), \end{aligned} \quad (36)$$

and, at first order in perturbation theory

$$S_n(t) - S_n(0) \approx \frac{1}{1-n} \frac{\langle \Omega | \mathcal{T}_n(0, t) | \Omega \rangle - \langle \Omega | \mathcal{T}_n(0, 0) | \Omega \rangle}{\langle \Omega | \mathcal{T}_n(0, 0) | \Omega \rangle}. \quad (37)$$

The quantity $\langle \Omega | \mathcal{T}_n(0, 0) | \Omega \rangle_{\text{post}}$, appearing on the RHS of (34) can be also expanded in a power series of δ_λ . From dimensional analysis and the mass-coupling relation (1) we have that

$$\tau_n = \langle \Omega | \mathcal{T}_n(0, 0) | \Omega \rangle = A_{\mathcal{T}_n} \lambda_2^{\frac{\Delta\mathcal{T}_n}{2-\Delta_\sigma}}, \quad (38)$$

where $A_{\mathcal{T}_n}$ is a non-universal function of n . Similarly

$$\langle \Omega | \mathcal{T}_n(0, 0) | \Omega \rangle_{\text{post}} = A_{\mathcal{T}_n} (\lambda_2 + \delta_\lambda)^{\frac{\Delta\mathcal{T}_n}{2-\Delta_\sigma}} = \tau_n \left(1 + \frac{\delta_\lambda}{\lambda_2} \frac{\Delta\mathcal{T}_n}{2-\Delta_\sigma} + \mathcal{O}(\delta_\lambda^2) \right). \quad (39)$$

From (39) and (34) it then follows at first order in δ_λ

$$\begin{aligned} S_n(t) - S_n(0) &\approx \frac{1}{1-n} \frac{\delta_\lambda}{\lambda_2} \frac{\Delta\mathcal{T}_n}{2-\Delta_\sigma} + \frac{\delta_\lambda n}{1-n} \sum_{a=1}^8 \frac{2}{m_{0,a}^2} F_a^\sigma \hat{F}_a^{\mathcal{T}_n} \cos(m_a t) \\ &+ \frac{2\delta_\lambda n}{1-n} \sum_{a,b=1}^8 \int_{-\infty}^{\infty} \frac{dp_a dp_b}{2\pi e_a e_b} \frac{\delta(p_a + p_b)}{e_a + e_b} \text{Re} \left[[F_{ab}^\sigma(p_a, p_b)]^* \hat{F}_{ab}^{\mathcal{T}_n}(p_a, p_b) [e^{-i(\tilde{e}_a + \tilde{e}_b)t}] \right] + \dots, \end{aligned} \quad (40)$$

where the form factors of the twist field are normalized by the pre-quench vacuum expectation value τ_n . Analogously, we can normalize the σ form factors by the pre-quench expectation value $\bar{\sigma}$ introduced earlier. Generally, this expectation value has the form $\bar{\sigma} = A_\sigma \lambda_2^{\frac{\Delta_\sigma}{2-\Delta_\sigma}}$, where A_σ is a known constant. Expressing the masses $m_{0,a}$ in the denominators of Eq. (40) in terms of the coupling as well (i.e. recalling Eq. (1)) we end up with

$$\begin{aligned} S_n(t) - S_n(0) &= \frac{1}{1-n} \frac{\delta_\lambda}{\lambda_2} \left[\frac{\Delta\mathcal{T}_n}{2-\Delta_\sigma} + n \mathcal{C}_\sigma \sum_{a=1}^8 \frac{2}{r_a^2} \hat{F}_a^\sigma \hat{F}_a^{\mathcal{T}_n} \cos(m_a t) \right. \\ &\left. + 2n \mathcal{C}_\sigma \sum_{a,b=1}^8 \int_{-\infty}^{\infty} \frac{dp_a dp_b}{2\pi e_a e_b} \frac{\delta(\hat{p}_a + \hat{p}_b)}{\hat{e}_a + \hat{e}_b} \text{Re} \left[[\hat{F}_{ab}^\sigma(p_a, p_b)]^* \hat{F}_{ab}^{\mathcal{T}_n}(p_a, p_b) e^{-i(\tilde{e}_a + \tilde{e}_b)t} \right] + \dots \right] + \mathcal{O}(\delta_\lambda^2), \end{aligned} \quad (41)$$

where

$$\mathcal{C}_\sigma = \frac{A_\sigma}{\kappa^2}, \quad (42)$$

is constant featuring in Eq. (9) of the Letter, κ is given in Eq. (1), $A_\sigma = -1.277(2)$ has been determined for instance in [10], r_a are the normalized masses defined earlier, and \hat{e}_a and \hat{p}_a are the relativistic energies and momentums (see below Eq. (2)) divided by the mass $m_{0,1}$. The ellipsis denotes higher particle number terms that are still first order in δ_λ .

In the E_8 minimal Toda field theory the (post-quench) particle masses are such that $m_5 > m_1 + m_2 > m_4 > 2m_1$. For this reason, oscillations coming from the two-particle form factor involving only particle types one and two, will have smaller frequency than those coming from the one-particle form factors of particle type five. Therefore, the six contributions to our expansion which involve the six smallest oscillation frequencies are precisely those coming from the form factors we have reviewed above. It is against these six contributions, that we have compared our numerical results in the Letter. More explicitly, expressing everything in terms of rapidities they are

$$\begin{aligned} S_n(t) - S_n(0) &= \frac{1}{1-n} \frac{\delta_\lambda}{\lambda_2} \left[\frac{\Delta_{\mathcal{T}_n}}{2 - \Delta_\sigma} + n \mathcal{C}_\sigma \sum_{a=1}^4 \frac{2}{r_a^2} \hat{F}_a^\sigma \hat{F}_a^{\mathcal{T}_n} \cos(r_a m_1 t) \right] \\ &+ 2n \mathcal{C}_\sigma \int_{-\infty}^{\infty} \frac{d\theta}{2\pi} \frac{1}{2 \cosh^2 \theta} \operatorname{Re} \left[[\hat{F}_{11}^\sigma(2\theta)]^* \hat{F}_{11}^{\mathcal{T}_n}(2\theta) e^{-2im_1 t \cosh \theta} \right] \\ &+ 2n \mathcal{C}_\sigma \int_{-\infty}^{\infty} \frac{d\theta}{2\pi} \frac{1}{\cosh \theta (\cosh \theta + r_2 \cosh \tilde{\theta})} \\ &\times \operatorname{Re} \left[[\hat{F}_{12}^\sigma(\theta - \tilde{\theta})]^* \hat{F}_{12}^{\mathcal{T}_n}(\theta - \tilde{\theta}) e^{-im_1 t (\cosh \theta + r_2 \cosh \tilde{\theta})} \right] + \dots \Big] + \mathcal{O}(\delta_\lambda^2), \end{aligned} \quad (43)$$

where

$$\tilde{\theta} := -\sinh^{-1} \left(\frac{\sinh \theta}{r_2} \right). \quad (44)$$

The limit $n \rightarrow 1$ needed to compute the von Neumann entropy can also be performed with the results given in the previous sections. For instance, for the one-particle form factor contributions, we just need to replace the form factors with the functions g_i defined in (5). This formula will give oscillatory terms of frequencies $m_1, m_2, m_3, 2m_1, m_4$ and $m_1 + m_2$ and can easily be evaluated numerically. Terms coming from the one-particle form factor contributions give undamped oscillations, whereas contributions from two-particle form factors, will produced damped oscillations, similar to those found in [4] for a different quench. For large t it is possible to extract the leading oscillatory part of the two-particle form factor contributions by stationary phase analysis. These terms are suppressed as $t^{-3/2}$.

Finally, the variation of the expectation value of the spin field after the quench can also be obtained by the same techniques and the expression is almost identical to (34)

$$\begin{aligned} \langle \Omega | \sigma(0, t) | \Omega \rangle - \bar{\sigma} &= \bar{\sigma} \frac{\delta_\lambda}{\lambda_2} \left[\frac{\Delta_\sigma}{2 - \Delta_\sigma} + \mathcal{C}_\sigma \sum_{a=1}^8 \frac{2}{r_a^2} |\hat{F}_a^\sigma|^2 \cos(m_a t) \right] \\ &+ 2\mathcal{C}_\sigma \sum_{a,b=1}^8 \int_{-\infty}^{\infty} \frac{dp_a dp_b}{2\pi e_a e_b} \frac{\delta(\hat{p}_a + \hat{p}_b)}{\hat{e}_a + \hat{e}_b} |\hat{F}_{ab}^\sigma(p_a, p_b)|^2 \cos((\tilde{e}_a + \tilde{e}_b)t) + \dots \Big] + \mathcal{O}(\delta_\lambda^2). \end{aligned} \quad (45)$$

In Fig. 3 we compare the numerical results for the one-point function of $\sigma(0, t)$ against the analytical formula (45), incorporating the first four one-particle and the first two two-particle contributions.

2 Transverse Field Quench: Mass Quench in Ising Field Theory

Considering the Ising field theory with $\lambda_2 = 0$, the model can be described by a free Majorana fermion with mass $m_0 = \lambda_1$. In [4] we presented a study of the evolution of entanglement after a mass quench in this model. As explained in [4], the linked cluster expansion of the quench one-point function developed in [11] generalizes to the branch point twist field as

$$\frac{\langle \Omega | \mathcal{T}_n(0, t) | \Omega \rangle}{\langle \Omega | \Omega \rangle} = \tilde{\tau}_n \sum_{k, l=0}^{\infty} D_{2k, 2l}(t), \quad (46)$$

where $|\Omega\rangle$ is the pre-quench vacuum expressed in the post-quench particle basis as recalled in Eq. (10) of the Letter, $\tilde{\tau}_n$ is the post-quench expectation value of the branch point twist field, $D_{2k, 2l}$ is the combination of the expansion coefficients

$$\langle \Omega | \mathcal{T}_n(0, t) | \Omega \rangle = \tilde{\tau}_n \sum_{k, l=0}^{\infty} C_{2k, 2l}(t), \quad (47)$$

and

$$\langle \Omega | \Omega \rangle = \sum_{q=0}^{\infty} Z_{2q}, \quad (48)$$

in the form

$$D_{2k, 2l}(t) = \sum_{p=0}^{\min(k, l)} \tilde{Z}_{2p} C_{2(k-p), 2(l-p)}(t), \quad (49)$$

and \tilde{Z}_{2p} is the inverse of Z_{2q} defined as $\sum_{q=0}^{\infty} Z_{2q} \cdot \sum_{p=0}^{\infty} \tilde{Z}_{2p} = 1$. In [4] we showed that (46) was in fact the expansion of the exponential of a Laurent expansion in powers of t , with highest power 1. Our proof however was only carried out for terms in the expansion of order K^2 where $K(\theta)$ is a known function that enters the definition of $C_{i, j}(t)$. Our aim here is to provide a complete proof of exponentiation. Namely, the statement that (46) is an exponential is a general one and can be shown at all orders in $K(\theta)$. The precise definitions are

$$\begin{aligned} \tilde{\tau}_n C_{2k, 2l}(t) &= \frac{1}{k!l!} \sum_{i_1, \dots, i_k=1}^n \sum_{j_1, \dots, j_l=1}^n \\ &\times \left[\prod_{s=1}^k \int_0^{\infty} \frac{d\theta'_s}{2\pi} K(\theta'_s)^* e^{2itE(\theta'_s)} \right] \left[\prod_{r=1}^l \int_0^{\infty} \frac{d\theta_r}{2\pi} K(\theta_r) e^{-2itE(\theta_r)} \right] \\ &\times {}_{n; i_1 i_1 \dots i_k i_k} \langle \theta'_1, -\theta'_1, \dots, \theta'_k, -\theta'_k | \mathcal{T}_n(0, 0) | -\theta_l, \theta_l, \dots, -\theta_1, \theta_1 \rangle_{j_1 j_1 \dots j_l j_1; n}, \end{aligned} \quad (50)$$

and

$$\begin{aligned} Z_{2q} &= \frac{1}{(q!)^2} \sum_{i_1, \dots, i_q=1}^n \sum_{j_1, \dots, j_q=1}^n \left[\prod_{s=1}^q \int_0^{\infty} \frac{d\theta'_s d\theta_s}{(2\pi)^2} K(\theta'_s)^* K(\theta_s) \right] \\ &\times {}_{i_1 i_1 \dots i_q i_q} \langle \theta'_1, -\theta'_1, \dots, \theta'_q, -\theta'_q | -\theta_q, \theta_q, \dots, -\theta_1, \theta_1 \rangle_{j_q j_q \dots j_1 j_1} \quad \text{for } q > 0, \end{aligned} \quad (51)$$

with $Z_0 = 1$. Combining the form of the expansion with the properties of the form factors such as the crossing relation and the Pfaffian nature of the multi-particle form factors (see [4] for

details), a ‘‘connected’’ expansion for the coefficients $C_{2k,2l}(t)$ and Z_{2q} is suggested which reads

$$C_{2k,2l}(t) = \sum_{\{n_{i,j}\}}^{k,l} \prod_{i,j=0}^{\infty} \frac{\left(C_{2i,2j}^c(t)\right)^{n_{i,j}}}{n_{i,j}!}, \quad (52)$$

$$Z_{2q} = \sum_{\{\tilde{n}_j\}}^q \prod_{j=0}^{\infty} \frac{\left(Z_{2j}^c\right)^{\tilde{n}_j}}{\tilde{n}_j!}, \quad (53)$$

where the summations go for non-negative integer partitions satisfying the constraints $\sum_{i,j=0}^{\infty} i n_{i,j} = k$, $\sum_{i,j=0}^{\infty} j n_{i,j} = l$, and $\sum_{i=0}^{\infty} i \tilde{n}_i = q$.

The inverse coefficients \tilde{Z}_{2k} also admit a connected expansion

$$\tilde{Z}_{2p} = \sum_{\{\tilde{m}_i\}}^p \prod_{i=0}^{\infty} \frac{\left(-Z_{2i}^c\right)^{\tilde{m}_i}}{\tilde{n}_i!}, \quad (54)$$

with the constraint $\sum_{j=0}^{\infty} j \tilde{m}_j = p$, that we show by evaluating the inverse relation

$$\sum_{q=0}^{\infty} Z_{2q} \cdot \sum_{p=0}^{\infty} \tilde{Z}_{2p} = \sum_{q=0}^{\infty} \sum_{\{\tilde{n}_i\}}^q \prod_{i=0}^{\infty} \frac{\left(Z_{2i}^c\right)^{\tilde{n}_i}}{\tilde{n}_i!} \cdot \sum_{p=0}^{\infty} \sum_{\{\tilde{m}_j\}}^p \prod_{j=0}^{\infty} \frac{\left(-Z_{2j}^c\right)^{\tilde{m}_j}}{\tilde{m}_j!}. \quad (55)$$

Let us reorganize the terms and group them according to number of the function K , i.e. according to the value $\Delta = k + p$

$$\sum_{\Delta=0}^{\infty} \sum_{k=0}^{\Delta} \sum_{\{\tilde{n}_i\}}^k \prod_{i=0}^{\infty} \frac{\left(Z_{2i}^c\right)^{\tilde{n}_i}}{\tilde{n}_i!} \sum_{\{\tilde{m}_j\}}^{\Delta-k} \prod_{j=0}^{\infty} \frac{\left(-Z_{2j}^c\right)^{\tilde{m}_j}}{\tilde{m}_j!}. \quad (56)$$

The sum of the integer partitions $\{\tilde{n}_i\}$ and $\{\tilde{m}_j\}$ can be seen as a new partition $\{\tilde{s}_i\}$ with constraint $\sum_{i=0}^{\infty} i \tilde{s}_i = \Delta$ that suggest further reorganization of the series to

$$\sum_{\Delta=0}^{\infty} \sum_{\{\tilde{s}_i\}}^{\Delta} \prod_{i=0}^{\infty} \sum_{t_i=0}^{\tilde{s}_i} \frac{\left(Z_{2i}^c\right)^{t_i}}{t_i!} \frac{\left(-Z_{2i}^c\right)^{\tilde{s}_i-t_i}}{\left(\tilde{s}_i-t_i\right)!}, \quad (57)$$

that, according to the binomial theorem, is nothing else but

$$\sum_{\Delta=0}^{\infty} \sum_{\{\tilde{s}_i\}}^{\Delta} \prod_{i=0}^{\infty} \frac{\left[Z_{2i}^c - Z_{2i}^c\right]^{\tilde{s}_i}}{\tilde{s}_i!} = 1, \quad (58)$$

proving the connected expansion of the inverse coefficients.

Examining the connected coefficients $C_{2k,2l}^c(t)$, we see that only diagonal terms, where $k = l$, are singular, since the successive application of the crossing relation leads to $C_{2k,2k}^c(t) \sim Z_{2k}^c$ in these cases. To have these singularities visible, we reorganize the expansion for $C_{2k,2l}(t)$ into product of diagonal and non-diagonal coefficients as

$$C_{2k,2l} = \sum_{p=0}^{\min(k,l)} \left[\sum_{\{\tilde{m}_i\}}^p \prod_{i=0}^{\infty} \frac{\left(C_{2i,2i}^c\right)^{\tilde{m}_i}}{\tilde{m}_i!} \right] \left[\sum_{\substack{\{n_{i,j}\} \\ i \neq j}}^{k-p,l-p} \prod_{i,j=0}^{\infty} \frac{\left(C_{2i,2j}^c\right)^{n_{i,j}}}{n_{i,j}!} \right]. \quad (59)$$

Plugging this back to (49) combining with (54) leads to

$$D_{2k,2l} = \sum_{q=0}^{\min(k,l)} \sum_{p=0}^{\min(k-q,l-q)} \left[\sum_{\{\tilde{n}_i\}}^q \prod_{i=0}^{\infty} \frac{(-Z_{2i}^c)^{\tilde{n}_i}}{\tilde{n}_i!} \right] \quad (60)$$

$$\times \left[\sum_{\{\tilde{m}_i\}}^p \prod_{i=0}^{\infty} \frac{(C_{2i,2i}^c)^{\tilde{m}_i}}{\tilde{m}_i!} \right] \left[\sum_{\substack{\{n_{ij}\} \\ i \neq j}}^{k-q-p,l-q-p} \prod_{i,j=0}^{\infty} \frac{(C_{2i,2j}^c)^{n_{ij}}}{n_{ij}!} \right]. \quad (61)$$

Introducing the variable $\Lambda = p + q$ we can rearrange the expression to

$$D_{2k,2l} = \sum_{\Lambda=0}^{\min(k,l)} \left\{ \sum_{r=0}^{\Lambda} \left[\sum_{\{\tilde{n}_i\}}^r \prod_{i=0}^{\infty} \frac{(-Z_{2i}^c)^{\tilde{n}_i}}{\tilde{n}_i!} \right] \left[\sum_{\{\tilde{m}_i\}}^{\Lambda-r} \prod_{i=0}^{\infty} \frac{(C_{2i,2i}^c)^{\tilde{m}_i}}{\tilde{m}_i!} \right] \right\} \quad (62)$$

$$\times \left[\sum_{\substack{\{n_{ij}\} \\ i \neq j}}^{k-\Lambda,l-\Lambda} \prod_{i,j=0}^{\infty} \frac{(C_{2i,2j}^c)^{n_{ij}}}{n_{ij}!} \right]. \quad (63)$$

By a similar argument as above, we can argue that the terms inside the curly bracket evaluate to

$$\sum_{\{\tilde{s}_i\}}^{\Lambda} \prod_{i=0}^{\infty} \frac{(C_{2i,2i}^c - Z_{2i}^c)^{\tilde{s}_i}}{\tilde{s}_i!}. \quad (64)$$

The combinations $D_{2i,2i}^c = C_{2i,2i}^c - Z_{2i}^c$ are regular, so are $D_{2i,2j}^c = C_{2i,2j}^c$ for $i \neq j$, hence the $D_{2k,2l}(t)$ also admits a connected expansion that is regular in the form

$$D_{2k,2l} = \sum_{\{n_{ij}\}}^{k,l} \prod_{i,j=0}^{\infty} \frac{(D_{2i,2j}^c)^{n_{ij}}}{n_{ij}!}. \quad (65)$$

Combining this with (46) leads to the proof of the exponential form of the one-point function

$$\frac{\langle \Omega | \mathcal{T}_n(0, t) | \Omega \rangle}{\langle \Omega | \Omega \rangle} = \tilde{\tau}_n \exp \left[\sum_{k,l=0}^{\infty} D_{2k,2l}^c \right]. \quad (66)$$

In the proof we did not use any special property of the branch point twist field form factors other than the crossing relation and the Pfaffian structure for the multi-particle form factors. These are true for other local operators as well, such as the spin field σ , hence we showed the full exponentiation of the one-point function of such operators too.

3 Numerical Results

The numerics in the present work were done using the infinite time evolving block decimation algorithm (iTEBD) [12, 13]. Exploiting translational invariance, a general many-body state can be approximated by a matrix product state (written in the canonical form)

$$|\Psi\rangle = \sum_{\dots, s_j, s_{j+1}, \dots} \dots \Lambda_o \Gamma_o^{s_j} \Lambda_e \Gamma_e^{s_{j+1}} \dots |\dots, s_j, s_{j+1}, \dots\rangle, \quad (67)$$

where $\Gamma_{e/o}^s$ are $\chi \times \chi$ matrices associated with the even/odd lattice sites, $\Lambda_{e/o}$ are diagonal $\chi \times \chi$ matrices, with singular values λ_i corresponding to the bipartition of the system along even/odd bonds. The value of χ is the bond dimension. Expectation values of local operators can be calculated with standard tensor contraction procedures. The singular values on the bonds are the Schmidt coefficients corresponding to the bipartition, meaning that they are the eigenvalues of the reduced density matrix, therefore the entropies can be easily calculated.

The simulation is based on the available code [14]. In our adaptation, both for finding the initial state (pre-quench ground state) using imaginary time evolution, and for the real time evolution we used a fourth order Suzuki–Trotter decomposition [15] of the time evolution operator. For the imaginary time evolution, the time step was set to $\tau = 0.0005$ and we applied $N = 200000$ Trotter steps, starting the iteration from the fully polarized state. For the post quench real time evolution the time step was set to $\delta t = 0.005$. We kept singular values $\lambda_i > 10^{-12}$ up to a maximal bond dimension which was set to $\chi_{max} = 300$. Due to the suppression of the entanglement growth shown in Fig. 2 this was sufficient to carry out the simulations. We used the same bond dimension for different couplings. As one gets closer to the critical point the von Neumann entropy of the initial state is expected to grow logarithmically with the inverse mass. This was perfectly captured by our simulation that justifies the choice for the maximal bond dimension. We can also conclude that the suppression of the entanglement growth is not due to truncation effects since states with higher entanglement are well approximated in our numerics. We run simulations close to the critical point with couplings $h_z = 1$ (the critical value) and $h_x = 0.0005, 0.001, 0.002, 0.003, 0.005$ for quenches with $\delta h_x/h_x = -0.04, 0.05$. The time dependent data has a leading frequency, corresponding to the mass of the lightest quasi-particle m . Due to dimensional analysis, rescaling the time with $m = \mathcal{B}_{lattice}(h_x + \delta h_x)^{8/15}$ one can plot the time signal in units of m^{-1} , i.e. all the time signals have “leading” frequency $\tilde{\omega} = 1$. For quenches with $\delta h_x/h_x = 0.05$ we obtained the fit $\mathcal{B}_{lattice} \approx 5.42553$, which was used for the $\delta h_x/h_x = -0.04$ quenches as well for consistency, leading to the same period. This procedure is summarized in Fig. 1 for the magnetization. In Fig. 2 we show the result of the rescaling for the von Neumann entropy.

Once all the curves are scaled together, we approximate the data with interpolating curves. This allows us to extrapolate to the scaling limit $h_x \rightarrow 0$ up to $mt = 170$. In the extrapolation procedure, first we determine the mass for each h_x , clearly having $m \rightarrow 0$ for decreasing h_x . Together with the time rescaling, this can be also interpreted as sending the lattice spacing (a) to zero, with fixed field theoretical mass $m = 1$. The mass and the lattice spacing always come in dimensionless combinations. We claim that one can extrapolate to the scaling limit using the scaling functions $S_n(am) = \Delta \mathcal{T}_n / (1 - n) \log(am) + B(am)^{1/n} + S_{n,scal.lim.}$ for the entropies and $(\Delta \sigma / \bar{\sigma})(am) = \tilde{B}am + (\Delta \sigma / \bar{\sigma})|_{scal.lim.}$ for the magnetization for any value of mt as in the transverse field case, see [16, 17] and the Appendix of [4]. For the von Neumann entropy the prefactor of the logarithm term is $-c/6$, and the fit of our data leads to $c \approx 0.49$ for all times less or equal than $mt = 170$, and for both quenches studied. This is very close to the theoretical value $1/2$ which is a further indication that the maximal bond dimension applied

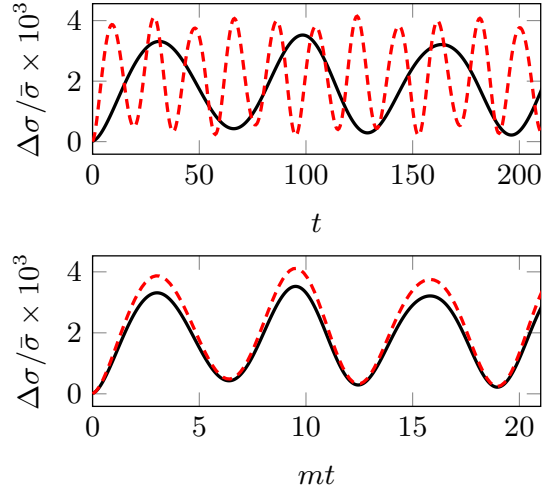


Figure 1: The rescaling and mass coupling relation fit, for a quench with $\delta h_x/h_x = 0.05$ for the magnetization difference $\Delta\sigma/\bar{\sigma} = \sigma(0, t)/\bar{\sigma} - 1$. Solid curves correspond to $h_x = 0.0005$ and dashed curves to $h_x = 0.005$. In the top plot the time is measured in “proper” time, based on the energy scale defined by the lattice Hamiltonian Eq.(1) in the Letter, therefore the curve of larger h_x (larger mass) has higher frequency oscillations. In the bottom we rescaled the time to be measured in units of m^{-1} , where $m \approx 5.42553(h_x + \delta h_x)^{8/15}$ to have the same frequency and allow for extrapolation.

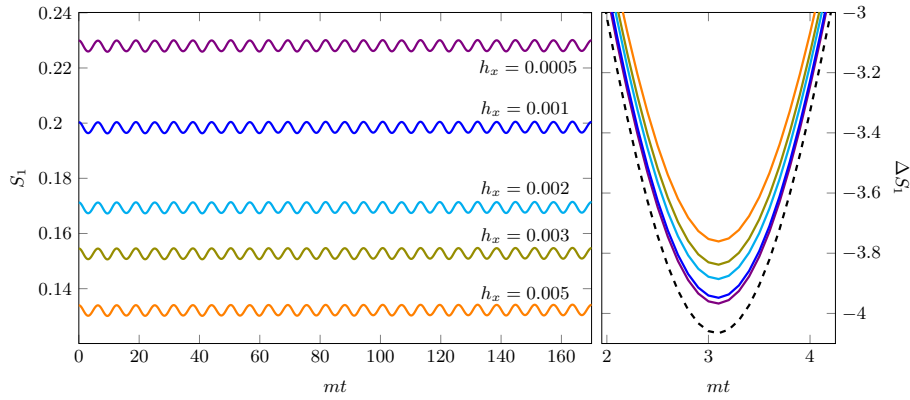


Figure 2: Left panel: Results of the rescaling for the von Neumann entropy for $\delta h_x/h_x = 0.05$. In the time frame we have simulation data for extrapolation, there is no visible trace of entanglement growth. The time is rescaled to be measured in units of m^{-1} , where $m \approx 5.42553(h_x + \delta h_x)^{8/15}$. Right panel: Demonstration of the change of ΔS_1 on a smaller time window, leading to convergence to the scaling limit. The colour of the curves denote the same h_x values as on the left panel. The dashed line is the extrapolated, scaling limit value of ΔS_1 , demonstrating the importance of calculating the scaling limit values to match the numerical data to the theoretical prediction.

was sufficient to capture the behaviour of the entanglement dynamics. For entropy differences between different times, the universal, time-independent logarithmic terms cancel, therefore we perform two parameter fits to extract the scaling limit values for ΔS_n . This process is displayed on the right hand side of Fig. 2 for the von Neumann entropy difference.

Additionally to the plots in the main text, here we plot our results for the initial time evolution of the magnetization in Fig. 3, and for the third and fourth Rényi entropies in Fig. 4. As in the main text for the von Neumann and the second Rényi entropies, we shifted the curves vertically by empirical values to compensate for possible higher order corrections that are constant in time. We comment on these contributions on the next Section and list the values of the shifts applied in Table 6.

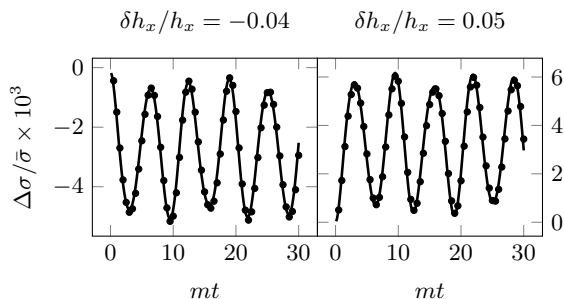


Figure 3: The time evolution of the magnetization for quenches with $\delta h_x/h_x = -0.04$ (left) and $\delta h_x/h_x = 0.05$ (right). The dots are the extrapolated iTEBD data. The lines are the theoretical predictions given in (45), incorporating the first four one-particle and the first two two-particle contributions.

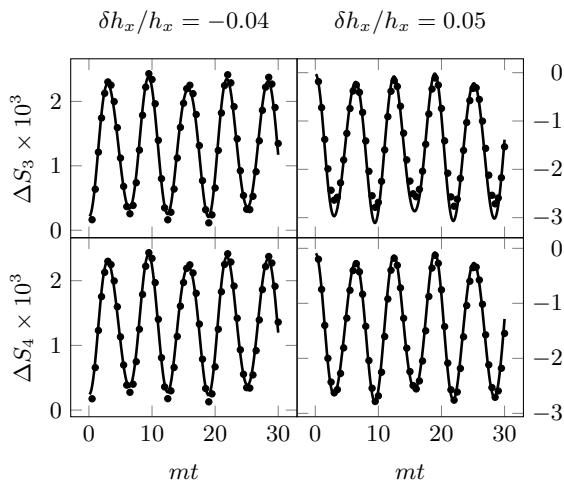


Figure 4: The time evolution of the 3rd (top) and 4th (bottom) Rényi entropies for quenches with $\delta h_x/h_x = 0.05$ (left) and $\delta h_x/h_x = -0.04$ (right). The dots are the extrapolated iTEBD data. The lines are the theoretical predictions given in (43), incorporating the first four one-particle and the first two two-particle contributions.

$\delta h_x/h_x = \delta_\lambda/\lambda_2$	\mathcal{D}_σ	$\tilde{\mathcal{D}}_\sigma$	\mathcal{D}_1	$\tilde{\mathcal{D}}_1$	\mathcal{D}_2	$\tilde{\mathcal{D}}_2$
-0.04	-0.00267	0.00005	0.00178	0.00015	0.00133	0.0001
0.05	0.00333	-0.00025	-0.00222	0.00015	-0.00167	0.00005
$\delta h_x/h_x = \delta_\lambda/\lambda_2$	\mathcal{D}_3	$\tilde{\mathcal{D}}_3$	\mathcal{D}_4	$\tilde{\mathcal{D}}_4$		
-0.04	0.00119	0.00015	0.00111	0.00025		
0.05	-0.00148	0	-0.00139	-0.0001		

Table 6: The empirical vertical shifts applied to $\Delta\sigma/\bar{\sigma}$ and ΔS_n to compensate for possible higher order corrections that are constant in time are denoted by $\tilde{\mathcal{D}}_\sigma$ and $\tilde{\mathcal{D}}_n$ respectively. As comparison, we also list the value of the first order constant terms coming from the change of the expectation values in (45) and (40), and we denoted them by $\mathcal{D}_\sigma = \delta_\lambda/\lambda_2 \cdot \Delta\sigma/(2 - \Delta_\sigma)$ and $\mathcal{D}_n = \delta_\lambda/\lambda_2 \cdot \Delta\mathcal{T}_n/(2 - \Delta_\sigma)/(1 - n)$. The applied shifts are one order of magnitude smaller than the first order result, in agreement with the expectation.

4 Beyond First Order Perturbation Theory

Finally we present some remarks on the suppression of linear growth and the constant in time shifts beyond first order perturbation theory.

First of all we comment on the empirical vertical shifts applied to our results summarized in Table 6. The vertical offset is related to corrections to the VEV of local operators given in Eq. (39) up to the first order. However there are higher order corrections to the VEVs. These second order corrections were calculated for the transverse field Ising quench in [4], and their magnitude is one order smaller to the first order values. Calculating the second order corrections to the offset for the longitudinal quench is an open problem beyond the scope of this paper, hence they were calibrated by hand to match the numerical data to the theoretical prediction. The magnitudes of these additional offsets compared to the first order results are one order smaller, as expected from the results of [4].

In [18], a perturbative expansion for the pre-quench state $|\Omega\rangle$ was determined in the eigenstates of the post-quench Hamiltonian H_{post} for the E_8 field theory up to $\mathcal{O}(\delta_\lambda^2)$; cf. Eq. (4) of our Letter. Of particular importance to estimate the rate of entanglement growth are the overlaps of pairs with zero momentum [19]

$$K_{ab}(\theta) := {}_{\text{post};a,b}\langle\theta, -\theta|\Omega\rangle; \quad a, b = 1, \dots, 8. \quad (68)$$

An interesting feature of these functions can be inferred from plots presented in Section 4 of [18]. One observes that the value of $|K_{11}(\theta_\star)|$ where θ_\star is the value of θ for which $|K_{11}(\theta)|$ is maximal, is of order 10^{-3} for $\delta_\lambda/\lambda_2 = 0.05$. In addition, $|K_{11}(\theta)|$ represents the largest particle overlap, so the maxima of other functions $K_{ab}(\theta)$ where a, b are not both 1, are generally at least one order of magnitude smaller. If we compare these orders of magnitude with the same values for the function $|K(\theta)|$ involved in the study of the Ising field theory mass quench [11], we see that $|K(\theta_\star)| \approx 10^{-2}$ for the same relative quench parameter, so roughly one order of magnitude larger. Since both the entanglement slope [4] and the higher order mass corrections [20] are expected to be proportional to $|K_{ab}(\theta)|^2$, for small quenches in the E_8 field theory, they are small and not visible on the timescales accessible with iTEBD. In order to further support these claims we have run an additional simulation for a quench of $h_x = 0.005$, $\delta h_x = 0.005$ and very large times. The resulting time evolution is plotted in Fig. 5. The time rescaling was carried out

using the same mass coupling relation as for small quenches. In this way the smallest frequency of the oscillations is close to one, within the resolution provided by the finite time window. This implies that even for a large quench, $\delta h_x/h_x = 1$, renormalization of the frequencies is absent. It is worth mentioning that the amplitudes of the oscillations are not predictable from a first order perturbative calculation. However, the numerical results certainly suggest that the oscillations in the entanglement entropy are not suppressed by higher order in perturbation theory. It is hard to assess whether the entropy will eventually grow linearly at large time from the numerical data, though failure to relax toward equilibrium is clear. Finally we note that there is a very low frequency modulation of the signal, which turns out to be related to the mass difference $2m_1 - m_3$: it originates from a second order contribution in perturbation theory, involving the operator matrix element between a one-particle state of particle 3 and a two-particle state of particle 1.

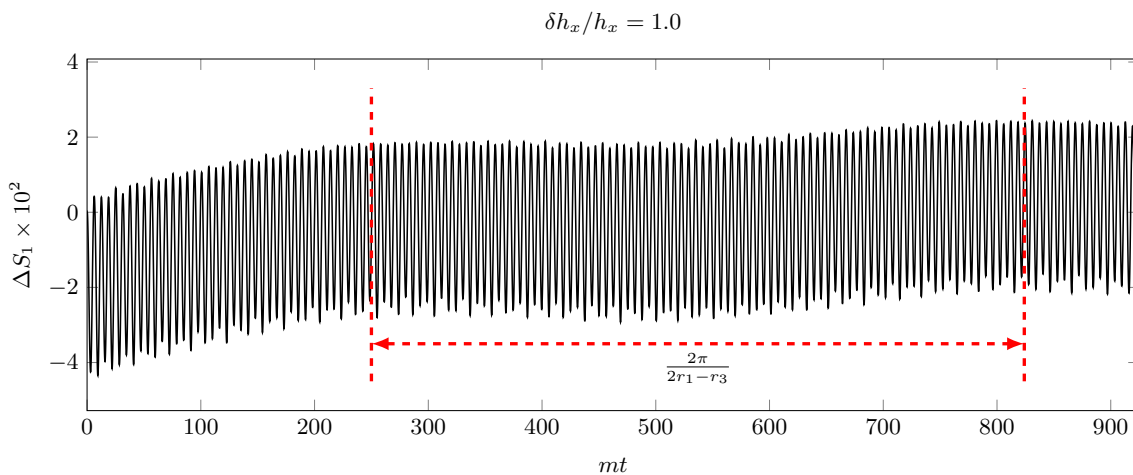


Figure 5: Time evolution of entanglement entropy for a large relative quench parameter $\delta h_x/h_x = 1$ with $h_x = 0.005$. The data suggest a slight drift in time of the entanglement entropy with oscillations present for large times as well. The low frequency modulation is related to the mass difference $2m_1 - m_3$ that is indicated by vertical dashed lines.

References

- [1] G. Delfino, Quantum quenches with integrable pre-quench dynamics, *J. Phys.* **A47**(40), 402001 (2014).
- [2] G. Delfino and J. Viti, On the theory of quantum quenches in near-critical systems, *J. Phys.* **A50**(8), 084004 (2017).
- [3] V. Fateev, The exact relations between the coupling constants and the masses of particles for the integrable perturbed conformal field theories, *Phys. Lett.* **B324**(1), 45–51 (1994).
- [4] O. A. Castro-Alvaredo, M. Lencsés, I. M. Szécsényi, and J. Viti, Entanglement Dynamics after a Quench in Ising Field Theory: A Branch Point Twist Field Approach, *JHEP* **2019**, 79 (2019).

- [5] A. B. Zamolodchikov, Integrable field theory from conformal field theory, *Adv. Stud. Pure Math.* **19**, 641–674 (1989).
- [6] A. B. Zamolodchikov, Integrals of Motion and S Matrix of the (Scaled) $T = T_c$ Ising Model with Magnetic Field, *Int. J. Mod. Phys.* **A4**, 4235 (1989).
- [7] O. A. Castro-Alvaredo, Massive Corrections to Entanglement in Minimal E_8 Toda Field Theory, *SciPost Phys.* **2**(1), 008 (2017).
- [8] G. Delfino and G. Mussardo, The Spin spin correlation function in the two-dimensional Ising model in a magnetic field at $T = T_c$, *Nucl. Phys.* **B455**, 724–758 (1995).
- [9] G. Delfino and P. Simonetti, Correlation functions in the two-dimensional Ising model in a magnetic field at $T = T_c$, *Phys. Lett.* **B383**, 450–456 (1996).
- [10] V. Fateev, S. L. Lukyanov, A. B. Zamolodchikov, and A. B. Zamolodchikov, Expectation values of local fields in Bullough-Dodd model and integrable perturbed conformal field theories, *Nucl. Phys.* **B516**, 652–674 (1998).
- [11] D. Schuricht and F. H. L. Essler, Dynamics in the Ising field theory after a quantum quench, *J. Stat. Mech.* **1204**, P04017 (2012).
- [12] G. Vidal, Efficient Simulation of One-Dimensional Quantum Many-Body Systems, *Phys. Rev. Lett.* **93**, 040502 (2004).
- [13] G. Vidal, Classical Simulation of Infinite-Size Quantum Lattice Systems in One Spatial Dimension, *Phys. Rev. Lett.* **98**, 070201 (2007).
- [14] F. Pollmann, Efficient Numerical Simulations Using Matrix-Product States, 2016.
- [15] E. Forest and R. D. Ruth, Fourth-order symplectic integration, *Physica* **43D**(1), 105 – 117 (1990).
- [16] P. Calabrese, J. Cardy, and I. Peschel, Corrections to scaling for block entanglement in massive spin-chains, *J. Stat. Mech.* **1009**, P09003 (2010).
- [17] J. Cardy and P. Calabrese, Unusual corrections to scaling in entanglement entropy, *J. Stat. Mech.* **2010**(4), 04023 (2010).
- [18] K. Hodsagi, M. Kormos, and G. Takacs, Perturbative post-quench overlaps in quantum field theory, *JHEP* **2019** (2019).
- [19] P. Calabrese and J. L. Cardy, Evolution of entanglement entropy in one-dimensional systems, *J. Stat. Mech.* **0504**, P04010 (2005).
- [20] K. Hodsagi, M. Kormos, and G. Takacs, Quench dynamics of the Ising field theory in a magnetic field, *SciPost Phys.* **5**, 27 (2018).